

Structure Preserving Diffusion Models

Haoye Lu*, Spencer Szabados*, and Yaoliang Yu

David R. Cheriton School of Computer Science
University of Waterloo, Ontario, Canada

Vector Institute, Ontario, Canada

{haoye.lu,sszabados,yaoliang.yu}@uwaterloo.ca

Abstract

Diffusion models have become the leading distribution-learning method in recent years. Herein, we introduce structure-preserving diffusion processes, a family of diffusion processes for learning distributions that possess additional structure, such as group symmetries, by developing theoretical conditions under which the diffusion transition steps preserve said symmetry. While also enabling equivariant data sampling trajectories, we exemplify these results by developing a collection of different symmetry equivariant diffusion models capable of learning distributions that are inherently symmetric. Empirical studies, over both synthetic and real-world datasets, are used to validate the developed models adhere to the proposed theory and are capable of achieving improved performance over existing methods in terms of sample equality. We also show how the proposed models can be used to achieve theoretically guaranteed equivariant image noise reduction without prior knowledge of the image orientation.

1 Introduction

Diffusion models (Song and Ermon 2019; Ho et al. 2020; Song et al. 2021a; Song et al. 2021b; Rombach et al. 2022; Karras et al. 2022; Song et al. 2023) have quickly become the leading method in a plethora of generative modelling tasks including image generation (Song and Ermon 2019; Ho et al. 2020; Song et al. 2021a), audio synthesis (Kong et al. 2021), image segmentation (Baranchuk et al. 2022; Wolleb et al. 2022) and image editing (Meng et al. 2022).

In many generation tasks, the data involved often exhibit inherent “structures” that result in their distributions remaining invariant – or the mappings between them being equivariant – under a set of transformations. For example, it is commonly assumed that the distribution of photographic images remains invariant under horizontal flipping. In tasks such as image denoising or inpainting, where the orientation of an image is not provided, it is natural to require the denoised or inpainted image to retain the same orientation as the input. Namely, the denoising or inpainting processes should exhibit equivariance under rotations and flipping.

Importantly, in certain critical applications, these properties are not merely desired but should be theoretically guaranteed to ensure consistency of the given model outputs or to prevent the introduction of additional biases or errors. A prime example can be found in the field of medical imaging analysis, where X-ray images are used to achieve diagnostic results. However, obtaining high-resolution X-ray scans often requires subjecting patients to higher doses of radiation, which presents a risk to patient safety (Goldman 2007; Huda 2002). Consequently, in order to improve patient safety, noise reduction techniques are critical to the use of lower resolution X-ray images by preserving image quality (Siemund et al. 2012). Moreover, given that medical

*These authors contributed equally to this work

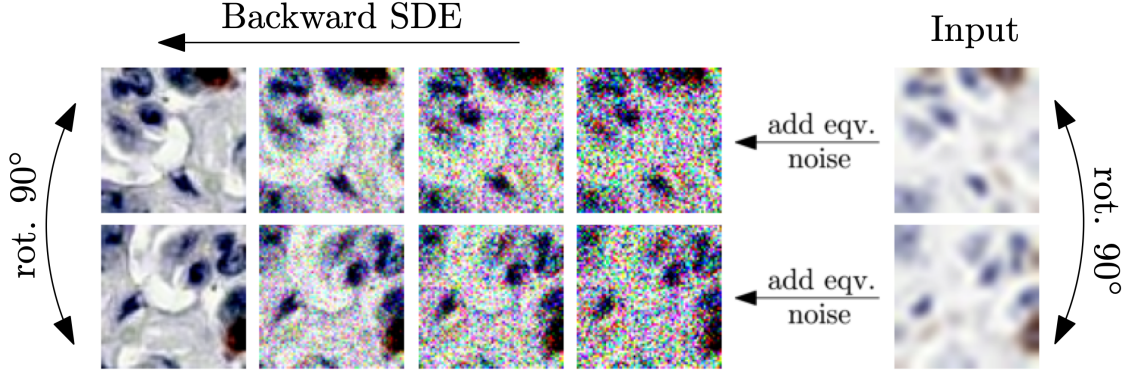


Figure 1: Ensuring Theoretical Equivariance: Denoising blurred images of LYSTO using SDEdit (Meng et al. 2022) without specifying input orientation; see Sec 6.3 for details. When rotating the input by 90° , the denoised output also rotates precisely by 90° .

images can be captured from a variety of different orientations (Lafarge et al. 2021; Shao et al. 2023), it is imperative such denoising techniques obey equivariant properties. This is in order to ensure consistent and reliable disease detection in the subsequent steps, regardless of the angle from which the images are obtained.

In this paper, we investigate *structure preserving diffusion processes* (SPDiff), a family of diffusion processes that preserve group-invariant properties of distributions. We show that a diffusion process qualifies as “structure-preserving” if and only if the transition between two infinitesimal steps is equivariant. Building upon these theoretical foundations, we introduce two novel methods that provide theoretically guaranteed capabilities for invariant data generation and equivariant data editing.

The first method, SPDiff+WT, relies on a weight-tied implementation, resulting in a lower training and sampling cost albeit with a trade-off in image quality. In contrast, the second method, SPDiff+OC, combines the outputs of diffusion models trained in a conventional manner to attain the same theoretical guarantees while achieving a sample quality comparable to that of a standard diffusion model. However, this last method incurs additional sampling costs, and we discuss approaches to mitigate this issue. Additionally, we propose a straightforward technique of incorporating a regularization term into existing diffusion models to promote invariant and equivariant properties.

We test the proposed methods on the rotated MNIST (Larochelle et al. 2007) and the LYSTO (Jiao et al. 2023) datasets, which respectively consist of rotated digits from the MNIST dataset (Deng 2012) and cell images whose distribution is naturally invariant under rotations and flipping. We also present how to use our method to implement an equivariant denoising algorithm as shown in Fig 1. The results corroborate our theoretical claims and provide additional insights.

2 Related work

The problem of conditioning neural networks to respect group-invariant (or equivariant) distributions (Shaw-Taylor 1993) has been a longstanding issue within the domains of physical modelling, computer vision, and, more recently, generative modelling. This is underscored by the widespread utilization of diverse forms of data augmentation, such as image illumination adjustments and orientation flipping/rotations, during the training process. Implicitly, these augmentation techniques symmetrize the underlying data distribution that the network is aiming to learn and represent an inductive prior imposed by the experimenters which may be deduced from prior domain knowledge of the task in question; e.g., rotation and mirror symmetries present in microscope slides and smears without a preferred orientation used in medical testing.

While data augmentation serves as a means of achieving approximate group invariance (or equivariance), relying solely on this approach necessitates an infinite number of training samples in order to guarantee the model is truly invariant. Consequently, models often fall short of being adequately conditioned through data augmentation alone Gao et al. 2022, and require more training data compared to conditioned models. As such a combination of other techniques becomes necessary to impose the required constraints when approximate invariance is not sufficient.

In the context of Convolutional Neural Networks (CNNs), there are several works that propose methods of constructing group-invariant CNNs for a selection of different groups (e.g., Cohen and Welling 2016; Esteves et al. 2018; Kondor and Trivedi 2018; Knigge et al. 2022) by formulating convolutional kernels and layer pooling operations that preserve the desired equivariance between layers of the network.

Recently, some work has appeared that focuses on conditioning Generative Adversarial Networks (GANs) Goodfellow et al. 2014; Goodfellow 2016 to obey generalized group equivariant properties inherent within the data distribution being learned Dey et al. 2021; Birrell et al. 2022. The first of which proposed a model by intuitively replacing all CNN layers within the GAN with group equivariant ones proposed in Cohen and Welling (2016). The resulting model was later argued to be incomplete by Birrell et al. (2022). This issue was addressed within the latter, which also proposed a set of invariant divergence measures.

Flow-based frameworks, which are more inherently related to diffusion than GANs, such as that proposed in Köhler et al. (2019), Köhler et al. (2020), Rezende et al. (2019), Liu et al. (2019), Biloš and Günnemann (2021), and Satorras et al. (2021) often make use of equivariant normalizing-flows to push-forward a group-invariant prior to the target distribution, which ensures the learned distribution is invariant.

To our knowledge, the study of group-invariance is underexplored for diffusion models Song and Ermon 2019; Song et al. 2021a; Ho et al. 2020; Karras et al. 2022; Kim et al. 2023, in particular neural models, outside the realm of molecular generation (i.e., molecular conformation generation) (Shi et al. 2021; Xu et al. 2022; Hooeboom et al. 2022). Where most approaches condition the diffusion process on a graph prior and employ a transformation (applied to the inner molecular atomic distances) that elevates the graph into a group-invariant form (or one that is more robust to the selected group transformations). Thereby, in a similar way to flow-based frameworks, as discussed in Albergo and Vanden-Eijnden (2023) and Albergo et al. (2023), this results in a representation that is sufficient (under parameterization assumptions) to ensure the diffusion process is equivariant.

3 Preliminary

3.1 The Diffusion Process

Let $\{\mathbf{x}_t\}_{t=0}^T$ denote a set of time-indexed random variables in \mathbb{R}^d such that $\mathbf{x}_t \sim p_t(\mathbf{x}_t)$, where $p_t(\mathbf{x}_t)$ are the marginal distributions induced by an underlying diffusion process, characterized by the solution to a stochastic differential equation (SDE) of the form:

$$d\mathbf{x}_t = \mathbf{f}(\mathbf{x}_t, t) dt + g(t) d\mathbf{w}_t, \quad \mathbf{x}_0 \sim p_0(\mathbf{x}_0), \quad (1)$$

where $\mathbf{f} : \mathbb{R}^d \times [0, T] \rightarrow \mathbb{R}^d$ is the *drift*, $g : [0, T] \rightarrow \mathbb{R}$ is a scalar *diffusion coefficient*, and $\mathbf{w}_t \in \mathbb{R}^d$ denotes a Wiener process. In generative diffusion models, we take $p_0 = p_{\text{data}}$ and $p_T = p_{\text{prior}}$; thereby, the diffusion process constructs a path from p_{data} to p_{prior} .

In practice, \mathbf{f} and g are chosen to accelerate the sampling of \mathbf{x}_t in Eq (1). In Table 1, we list two popular selections of \mathbf{f} and g , respectively corresponding to the variance preserving (VP) Ho et al. 2020; Song et al. 2021a and variance exploding (VE) SDEs Song et al. 2021b. Under these settings, given $\mathbf{x}_0 \sim p_0(\mathbf{x}_0)$, we have

$$\mathbf{x}_t \sim \mathcal{N}(\boldsymbol{\mu}_t \mathbf{x}_0, \sigma_t^2 \mathbf{I}). \quad (2)$$

Table 1: Typical choices of $\mathbf{f}(\mathbf{x}, t)$ and $g(\mathbf{x})$, where \mathbf{I} denotes the identity matrix. For VP-SDE (Ho et al. 2020; Song et al. 2021a), α_t is a differentiable decreasing function such that $\alpha_0 = 1$ and $\alpha_1 = 0$. For VE-SDE (Song et al. 2021b), σ_t^2 is strictly increasing with $\sigma_0^2 = 0$ and $\lim_{t \rightarrow \infty} \sigma_t^2 = \infty$.

SDE	$\mathbf{f}(\mathbf{x}, t)$	$g(t)$	$\boldsymbol{\mu}_t$	σ_t^2	T
VP	$\frac{1}{2} \frac{d \log \alpha_t}{dt} \mathbf{x}$	$\sqrt{-\frac{d \log \alpha_t}{dt}}$	$\sqrt{\alpha_t} \mathbf{I}$	$(1 - \alpha_t)$	1
VE	$\mathbf{0}$	$\sqrt{\frac{d[\sigma_t^2]}{dt}}$	\mathbf{I}	σ_t^2	∞

As a result, \mathbf{x}_t can be sampled using the reparameterization trick by simply picking $\mathbf{x}_0 \sim p_0(\mathbf{x}_0)$ and setting $\mathbf{x}_t = \boldsymbol{\mu}_t \mathbf{x}_0 + \sigma_t \boldsymbol{\epsilon}$, where $\boldsymbol{\epsilon} \sim \mathcal{N}(\mathbf{0}, \mathbf{I})$.

Remarkably, for any SDE, there exists a corresponding reverse SDE sharing the same marginal distribution p_t for all $t \in [0, T]$ Anderson 1982. In fact, for the forward SDE in Eq (1), there exists a family of reverse-time SDEs given by:

$$d\mathbf{x}_t = \left[\mathbf{f}(\mathbf{x}_t, t) - \frac{1 + \lambda^2}{2} g^2(t) \nabla_{\mathbf{x}_t} \log p_t(\mathbf{x}_t) \right] dt + \lambda g(t) d\mathbf{w}_t \quad (3)$$

for all $\lambda \geq 0$ (Zhang and Chen 2023).

Setting $\lambda = 1$ in Eq (3) simplifies to the original reverse SDE as derived by Anderson (1982). Likewise, for $\lambda = 0$, the process transforms into a deterministic ODE process, known as the probability flow ODE (PF-ODE) as described by Song et al. (2021b).

In Eq (3), the only unknown term is the score $\nabla_{\mathbf{x}} \log p_t(\mathbf{x})$, which can be estimated using a neural network $\mathbf{s}_\theta(\mathbf{x}, t)$ trained to minimize the score-matching loss (Song et al. 2021b):

$$\mathcal{L}(\theta) = \mathbb{E} \left[\left\| \mathbf{s}_\theta(\mathbf{x}_t, t) - \nabla_{\mathbf{x}_t} \log p(\mathbf{x}_t | \mathbf{x}_0) \right\|^2 \right] \quad (4)$$

where the expectation is taken over $t \sim \mathcal{U}(0, T)$, $\mathbf{x}_t \sim p(\mathbf{x}_t | \mathbf{x}_0)$, $\mathbf{x}_0 \sim p_{\text{data}}$. Subsequently, one can start from $\mathbf{x}_T \sim p_T(\mathbf{x}_T)$ and sample $\mathbf{x}_0 \sim p_{\text{data}}(\mathbf{x}_0)$ by solving the SDE (or ODE if $\lambda = 0$) given in Eq (3).

3.2 Group Invariance and Equivariance

A set of functions $\mathcal{G} = \{h : \mathcal{X} \rightarrow \mathcal{X}\}$ equip with a associative binary operation $\circ : \mathcal{G} \times \mathcal{G} \rightarrow \mathcal{G}$, composition in this case, is called a *group* if (1) for any $h_1, h_2 \in \mathcal{G}$, then $h_1 \circ h_2 \in \mathcal{G}$; (2) \mathcal{G} has an identity operator \mathbf{e} with $\mathbf{e} \circ h = h \circ \mathbf{e} = h$; and (3) for any $h \in \mathcal{G}$, there exists an inverse operator h^{-1} such that $h^{-1} \circ h = h \circ h^{-1} = \mathbf{e}$. For instance, let f_x be the operator that flips images horizontally. Then, $\mathcal{G} = \{f_x, \mathbf{e}\}$ is a group where $f_x^{-1} = f_x$.

In this paper, we are interested in sampling from a \mathcal{G} -invariant distribution with a smooth density function $p : \mathbb{R}^d \rightarrow \mathbb{R}^+$ that is non-zero everywhere.¹ Given a group \mathcal{G} , a distribution p is \mathcal{G} -invariant if for all closed ball $B \subseteq \mathbb{R}^d$ and $h \in \mathcal{G}$,

$$\int_B p(\mathbf{x}) d\mathbf{x} = \int_{h(B)} p(\mathbf{z}) d\mathbf{z}, \quad (5)$$

where $h(B) = \{h(\mathbf{x}) | \mathbf{x} \in B\}$. We restrict our discussion herein to *linear isometry*, which preserves distance in a sense that for all $\mathbf{x}, \mathbf{y} \in \mathbb{R}^d$ and $h \in \mathcal{G}_{\mathcal{L}}$, $\|h(\mathbf{x}) - h(\mathbf{y})\|_2 = \|\mathbf{x} - \mathbf{y}\|_2$.² This assumption excludes the ‘‘scaling’’ effect of h ; otherwise, as shown in example 1, the group-invariant $p(\mathbf{x})$ can only be non-zero at $\mathbf{x} = \mathbf{0}$, making the problem trivial and violating the previous strictly positive density assumption.

¹This assumption can be easily satisfied by adding a tiny Gaussian noise to a distribution.

²We use subscript \mathcal{L} to denote a group of linear isometries.

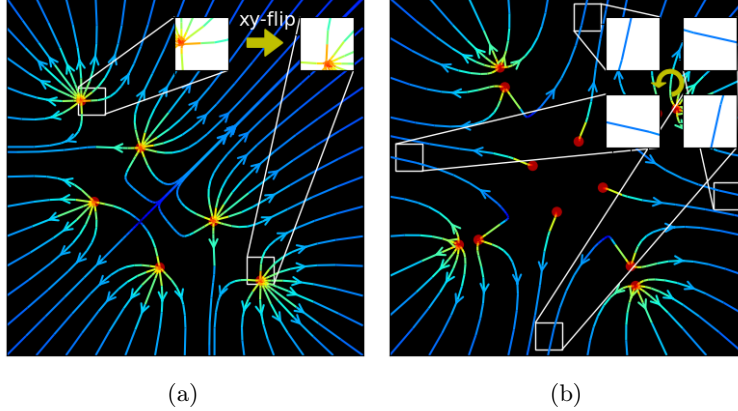


Figure 2: The vector fields of score functions that are equivariant under xy -flip (left) and $(90 \cdot k)^\circ$ rotation for $k = 0, 1, 2, 3$ (right).

Example 1 Consider a group $\mathcal{S} = \{a(\cdot) | a > 0\}$ consisting of all positive scaling functions defined on \mathbb{R} . Assume distribution p is \mathcal{S} -invariant. Pick $a > 1$ and let $I_n = [-a^{n+1}, -a^n] \cup [a^n, a^{n+1}]$ for $n \in \mathbb{Z}$. Then we have

$$\int_{I_n} p(x) dx = \alpha \geq 0 \quad (6)$$

for all $n \in \mathbb{Z}$. As $\{\{0\}\} \cup \{[-a^{n+1}, -a^n] \cup [a^n, a^{n+1}], n \in \mathbb{Z}\}$ is a cover of \mathbb{R} , the smooth p must be non-zero in at least one interval. (Otherwise, its integration on \mathbb{R} is zero instead of one, a contradiction.) If p is non-zero on I_n for some n , then $\alpha > 0$ and $\int_{\mathbb{R}} p(x) dx = \infty$, a contradiction. Hence, p can only be non-zero at $x = 0$, contradicting the assumption that p is smooth. For $a < 1$, we can get the same contradiction by picking its inverse a^{-1} .

As diffusion models learn a distribution by estimating its score, the following lemma shows if a distribution is $\mathcal{G}_{\mathcal{L}}$ -invariant, its score has to be $\mathcal{G}_{\mathcal{L}}$ -equivariant. (All the proofs can be found in appx A.)

Lemma 1 $p(\mathbf{x})$ is $\mathcal{G}_{\mathcal{L}}$ -invariant if and only if

$$\mathbf{s}(\mathbf{h}(\mathbf{x})) = D\mathbf{h}(\mathbf{x}) \mathbf{s}(\mathbf{x}) \quad (7)$$

for all $\mathbf{h} \in \mathcal{G}_{\mathcal{L}}$ and $\mathbf{x} \in \mathbb{R}^d$, where $\mathbf{s}(\mathbf{x})$ denotes the score function $\nabla_{\mathbf{x}} \log p(\mathbf{x})$ and $D\mathbf{h}$ the Jacobian matrix of \mathbf{h} .

To see how Lem 1 works, consider a group of linear isometries $\mathcal{G}_{\mathcal{L}}$ such that for $\mathbf{h} \in \mathcal{G}_{\mathcal{L}}$, we have $\mathbf{h}(\mathbf{x}) = A_{\mathbf{h}}\mathbf{x}$ for some $A_{\mathbf{h}} \in \mathbb{R}^{d \times d}$. Then Eq (7) becomes

$$\mathbf{s}(A_{\mathbf{h}}\mathbf{x}) = A_{\mathbf{h}} \mathbf{s}(\mathbf{x}), \quad (8)$$

and the lemma says the score function at $A_{\mathbf{h}}\mathbf{x}$ is the same as the one at \mathbf{x} transformed by $A_{\mathbf{h}}$. That is, for linear group isometries, $p(\mathbf{x})$ is $\mathcal{G}_{\mathcal{L}}$ -invariant if and only if the score \mathbf{s} commutes with all $\mathbf{h} \in \mathcal{G}_{\mathcal{L}}$.

In Fig 2, we illustrate this commutative relationship between invariant distributions when subjected to xy -flip and rotations, both of which are linear transformations. In Fig 2a, it is evident that when we select symmetric points relative to the diagonal $x = y$, the score at these two points also exhibits symmetry. This implies that we can obtain an identical score vector by either flipping a point and then computing its score or by evaluating its score first and subsequently applying the flip operation. Similarly, in Fig 2b, we can derive the score vector by either rotating a point about the origin and then evaluating its score or by evaluating its score first and subsequently applying the rotation operation.

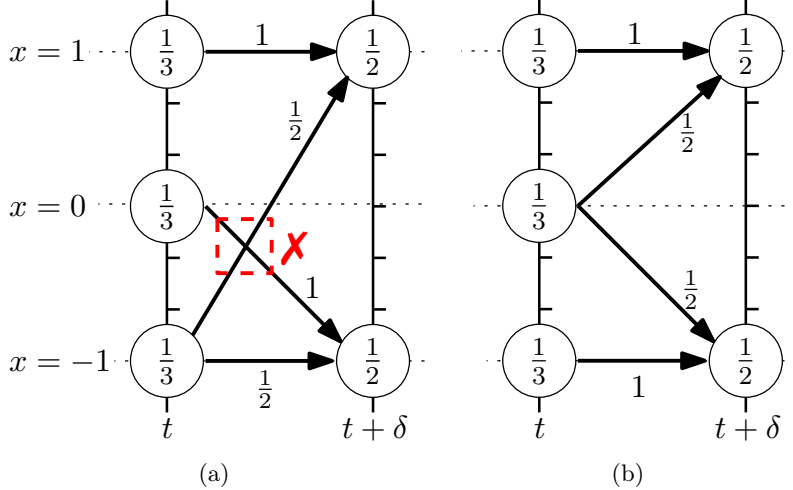


Figure 3: Two possible choices of the transition schemes between two discrete distributions p_t and $p_{t+\delta}$ that are invariant with respect to the flipping about $x=0$. Numbers in nodes and on edges represent marginal and transition probability, respectively. For diffusion processes, an intersection of transition paths, as shown in the left plot, is not possible as the transition in an infinitesimal step follows an optimal transport map (Khrukov et al. 2023).

4 Structure Preserving Diffusion Processes

In this section, we delve into the examination of diffusion processes that maintain the structure of the data distribution. Specifically, given a data distribution that is assumed $\mathcal{G}_{\mathcal{L}}$ -invariant, we explore the sufficient and necessary configurations of diffusion processes to preserve this invariance property for all $t \geq 0$. These insights will serve as a foundation for designing the corresponding score-matching neural networks in Sec 5.

Under the aforementioned weak assumptions (we also summarize all the assumptions in appx A), we present our main theoretical results in Prop 1:

Proposition 1 *Let $\mathcal{G}_{\mathcal{L}}$ be a group comprised of linear isometries on \mathbb{R}^d . Consider a diffusion process taking the form in Eq (1) with $\mathcal{G}_{\mathcal{L}}$ -invariant p_0 . Then, p_t is $\mathcal{G}_{\mathcal{L}}$ -invariant for all $t \geq 0$ if and only if*

$$Dh(\mathbf{x}) \mathbf{f}(\mathbf{x}, t) = \mathbf{f}(h(\mathbf{x}), t) \quad (9)$$

for all $t \geq 0$, $\mathbf{x} \in \mathbb{R}^d$ and $h \in \mathcal{G}_{\mathcal{L}}$.

Basically, the proposition tells us that a diffusion process retains the $\mathcal{G}_{\mathcal{L}}$ -invariance property of the data distribution p_0 throughout the trajectory if and only if its drift function is $\mathcal{G}_{\mathcal{L}}$ -equivariant. As a result, given a group $\mathcal{G}_{\mathcal{L}}$, we say a diffusion process is *structure preserving* if its drift term satisfies Eq (9).

To gain an intuitive understanding of why a $\mathcal{G}_{\mathcal{L}}$ -equivariant drift is sufficient, it's helpful to consider that the SDE in Eq (1) essentially describes the probability of \mathbf{x}_t transitioning to $\mathbf{x}_{t+\delta}$ at time t in an infinitesimal step δ . Therefore, an $\mathcal{G}_{\mathcal{L}}$ -equivariant drift term leads to an equivariant transition probability such that

$$p(\mathbf{x}_{t+\delta} = \mathbf{a} | \mathbf{x}_t = \mathbf{b}) = p(\mathbf{x}_{t+\delta} = h(\mathbf{a}) | \mathbf{x}_t = h(\mathbf{b})). \quad (10)$$

In essence, this implies that \mathbf{x}_t follows the same trajectory under transformations $h \in \mathcal{G}_{\mathcal{L}}$. Additionally, given that p_t is $\mathcal{G}_{\mathcal{L}}$ -invariant, the initial state distribution of \mathbf{x}_t remains unchanged when transformed by h .

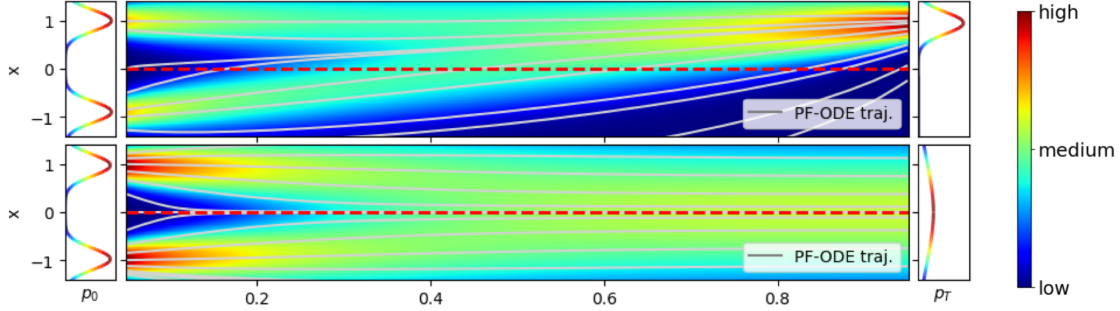


Figure 4: The evolution of p_t driven by diffusion processes where the data distribution p_0 is invariant under flipping with respect to the origin. We also plot the PF-ODE trajectories to visualize the transition direction of $p_t(x)$. The upper plot has $f(x, t) = \frac{1-x}{1-t}$ and $g(t) = 1$. The lower is the VP-SDE in table 1 with $\alpha_t = 1 - t$. For both processes, $T = 0.95$.

Consequently, the subsequent state distribution of $\mathbf{x}_{t+\delta}$ also remains invariant when transformed by h . This relationship can be applied recursively, starting from $t = 0$, to see why p_t remains $\mathcal{G}_{\mathcal{L}}$ -invariant for all $t \geq 0$.

Conversely, it's worth noting that a $\mathcal{G}_{\mathcal{L}}$ -invariant transition probability is not always necessary when dealing with discrete time steps. In Fig 3, we plot two possible choices for transitioning from the discrete distribution p_t to $p_{t+\delta}$, both of which are invariant under the flipping operation about the origin. For the first choice, Fig 3a, the transition is evidently not equivariant with respect to flipping. However, as the transition of diffusion processes in an infinitesimal step follows an optimal transport map (Khrukov et al. 2023), it becomes impossible for the transition paths to intersect in an infinitesimal step. This means the first choice, which is not equivariant, cannot occur in our configuration. In order to prevent intersections and ensure a valid transition scheme, the only viable option is the one depicted in Fig 3b, which is equivariant with respect to flipping.

In Fig 4, we visualize the evolution of p_t driven by two different diffusion processes with p_0 invariant to flipping with respect to $x = 0$ (i.e., $h(x) = -x$). Specifically, for the upper plot, we have drift $\mathbf{f}(x, t) = \frac{1-x}{1-t}$ that pushes x to 1 and is not flipping-equivariant for $t \geq 0$. As we observe, for all $t > 0$, p_t is no longer flipping-invariant, which corroborates Prop 1. For the second plot, we select the VP-SDE (see table 1) with $\alpha_t = 1 - t$ for $t \in (0, 1)$. Then its drift $\mathbf{f}(x, t) = -\frac{x}{2(1-t)}$ is equivariant to flipping as $\mathbf{f}(-x, t) = -\mathbf{f}(x, t)$. As suggested by the plot, p_t has a symmetric density for all $t \geq 0$, which is also aligned with Prop 1. Interestingly, this result can be generalized to all groups $\mathcal{G}_{\mathcal{L}}$ consisting of linear isometries and linear drifts such that $\mathbf{f}(\mathbf{x}, t) = \mathbf{x}f(t)$:

Corollary 1 *Assume the drift term takes the form $\mathbf{f}(\mathbf{x}, t) = \mathbf{x}f(t)$ for some scalar function $f : \mathbb{R} \rightarrow \mathbb{R}$. Then for any group $\mathcal{G}_{\mathcal{L}}$ composed of linear isometries, if p_t is $\mathcal{G}_{\mathcal{L}}$ -invariant at $t = 0$, then it is $\mathcal{G}_{\mathcal{L}}$ -invariant for all $t \geq 0$.*

Since the drift terms of both VP and VE-SDE, presented in table 1, take the form $\mathbf{x}f(t)$, Cor 1 tells us they are structure-preserving for arbitrary groups composed of linear isometries.

5 Structure Preserving Diffusion Models

In this section, we explore the application of the insights developed in Sec 4 to ensure the data generated by SPDif adheres to a $\mathcal{G}_{\mathcal{L}}$ -invariant distribution. Specifically, as mentioned in Sec 3, the sampling of a diffusion model involves solving the SDE in Eq (3) by estimating the score $\nabla_{\mathbf{x}} \log p_t(\mathbf{x})$ using a neural network $\mathbf{s}_{\theta}(\mathbf{x}, t)$.

We will discuss a few effective methods to design and train $\mathbf{s}_\theta(\mathbf{x}, t)$ so that it satisfies the properties required by SPDiff to achieve theoretically guaranteed $\mathcal{G}_\mathcal{L}$ -invariant sampling.

Leveraging the same neural network models, we subsequently explore a technique to inject “equivariant” noise in the resolution of Eq (3). This approach results in a theoretically assured equivariant trajectory and enables us to carry out equivariant data editing.

5.1 $\mathcal{G}_\mathcal{L}$ -nvariant Distribution Sampling

By Prop 1, when a diffusion process is structure preserving, p_t is $\mathcal{G}_\mathcal{L}$ -invariant for all $t \geq 0$. So, specifically, the prior distribution p_T is $\mathcal{G}_\mathcal{L}$ -invariant and by Lem 1, for all $t \geq 0$, the score $\nabla_{\mathbf{x}} \log p_t(\mathbf{x})$ is $\mathcal{G}_\mathcal{L}$ -equivariant. As a result, as long as the score estimator $\mathbf{s}_\theta(\mathbf{x}, t)$ perfectly learns the $\mathcal{G}_\mathcal{L}$ -equivariant property, the drift of reverse-time SDE Eq (3):

$$\tilde{\mathbf{f}}_{\theta, \lambda}(\mathbf{x}_t, t) = \mathbf{f}(\mathbf{x}_t, t) - \frac{1 + \lambda^2}{2} g^2(t) \mathbf{s}_\theta(\mathbf{x}, t) \quad (11)$$

is $\mathcal{G}_\mathcal{L}$ -equivariant. Applying Prop 1 with reversed t , we can then conclude that the generated samples must follow a $\mathcal{G}_\mathcal{L}$ -invariant distribution. Due to this observation, to ensure the generated data is sampled from a $\mathcal{G}_\mathcal{L}$ -invariant distribution, it is sufficient (and necessary) to train a $\mathcal{G}_\mathcal{L}$ -equivariant score estimator \mathbf{s}_θ .

Here, we present two theoretically guaranteed $\mathcal{G}_\mathcal{L}$ -equivariant implementations of \mathbf{s}_θ , SPDiff+WT and SPDiff+OC. Additionally, we also propose a regularizer, SPDiff+Reg, that can be directly added to the regular diffusion score-matching loss to improve the $\mathcal{G}_\mathcal{L}$ -equivariant property of \mathbf{s}_θ .

Weight Tying (SPDiff+WT). Currently, almost all existing diffusion models are based on the U-Net backbone (Salimans et al. 2017; Ronneberger et al. 2015). As the only components that are not equivariant are CNNs, we replace them with group-equivariant CNNs to make the entire network equivariant.

As we only consider linear isometry groups $\mathcal{G}_\mathcal{L}$, we can make the CNNs equivariant by tying the weights of its convolution kernel \mathbf{k} , which will also reduce the total number of parameters and improve the computation efficiency (Ravanbakhsh et al. 2017).³ We provide more details on our selections of weight-tied kernels for empirical study in appx B.

Output Combining (SPDiff+OC). The second method achieves $\mathcal{G}_\mathcal{L}$ -equivariance by leveraging the following fact: for any function $\mathbf{r} : \mathbb{R}^d \rightarrow \mathbb{R}^d$,

$$\tilde{\mathbf{r}}(\mathbf{x}) = \frac{1}{|\mathcal{G}_\mathcal{L}|} \sum_{\mathbf{h} \in \mathcal{G}_\mathcal{L}} A_{\mathbf{h}}^{-1} \mathbf{r}(A_{\mathbf{h}} \mathbf{x}) \quad (12)$$

is $\mathcal{G}_\mathcal{L}$ -equivariant, where $|\mathcal{G}_\mathcal{L}|$ denotes the number of elements in $\mathcal{G}_\mathcal{L}$ and $A_{\mathbf{h}}$ is the matrix such that $\mathbf{h}(\mathbf{x}) = A_{\mathbf{h}} \mathbf{x}$. (Derivation details are given in appx A.4.)

Based on this fact, we can obtain an equivariant estimator $\tilde{\mathbf{s}}_\theta(\cdot, t)$ of score $\nabla_{\mathbf{x}} \log p_t(\mathbf{x})$ by setting $\mathbf{r}(\cdot) = \mathbf{s}_\theta(\cdot, t)$, where \mathbf{s}_θ can be obtained through the regular score matching in Eq (4) with data augmentation that randomly applies group operator on \mathbf{x}_0 .

To see why $\tilde{\mathbf{s}}_\theta$ remains a valid estimator of $\nabla_{\mathbf{x}} \log p_t(\mathbf{x})$, note that the score matching makes $\mathbf{s}_\theta(\mathbf{x}, t) \approx \nabla_{\mathbf{x}} \log p_t(\mathbf{x})$. As the ground truth p_t is invariant, by Eq (8), $A_{\mathbf{h}}^{-1} \mathbf{s}_\theta(A_{\mathbf{h}} \mathbf{x}, t) \approx A_{\mathbf{h}}^{-1} \nabla_{A_{\mathbf{h}} \mathbf{x}} \log p_t(A_{\mathbf{h}} \mathbf{x}) = \nabla_{\mathbf{x}} \log p_t(\mathbf{x})$ for all $\mathbf{h} \in \mathcal{G}_\mathcal{L}$. Thus, the average

$$\tilde{\mathbf{s}}_\theta(\mathbf{x}, t) = \frac{1}{|\mathcal{G}_\mathcal{L}|} \sum_{\mathbf{h} \in \mathcal{G}_\mathcal{L}} A_{\mathbf{h}}^{-1} \mathbf{s}_\theta(A_{\mathbf{h}} \mathbf{x}, t), \quad (13)$$

³For general groups, readers may refer to the method by Cohen and Welling (2016) and Knigge et al. (2022) to make CNN \mathcal{G} -equivariant.

is also a valid estimator of $\nabla_{\mathbf{x}} \log p_t(\mathbf{x})$.

Compared to traditional diffusion models, this method changes the sampling process by combining multiple inference outputs of \mathbf{s}_θ to realize $\mathcal{G}_\mathcal{L}$ -equivariance. Importantly, the combination does not compromise the quality of the generated samples, as demonstrated in Sec 6. However, it does lead to an increase in the overall sampling cost. A potential approach to alleviating this problem is to distill the model by consistency models Song et al. 2023 combined with a weight-tying U-Net backbone. We leave this direction for future study.

Equivariance Regularization (SPDiff+Reg). Instead of achieving $\mathcal{G}_\mathcal{L}$ -equivariance by adopting model architectures, we can also directly add a regularizer to the score-matching loss to inject this preference. Specifically, according to Eq (8), the estimated score $\mathbf{s}_\theta(\cdot, t)$ is equivariant if

$$\mathbf{s}_\theta(A_h \mathbf{x}, t) = A_h \mathbf{s}_\theta(\mathbf{x}, t), \quad (14)$$

for all $h \in \mathcal{G}_\mathcal{L}$. Thus, we propose the following regularizer to encourage the two terms to match for all \mathbf{x} and t :

$$\mathcal{R}(\theta, \bar{\theta}) = \mathbb{E} \left[\frac{1}{|\mathcal{G}_\mathcal{L}|} \sum_{h \in \mathcal{G}_\mathcal{L}} \|\mathbf{s}_\theta(A_h \mathbf{x}, t) - A_h \mathbf{s}_{\bar{\theta}}(\mathbf{x}, t)\|^2 \right] \quad (15)$$

where the expectation is taken over the same variables in Eq (4) and $\bar{\theta}$ denotes the exponential moving average (EMA) of the model weights

$$\bar{\theta} \leftarrow \text{stopgrad}(\mu \bar{\theta} + (1 - \mu) \theta) \quad \text{with } \mu \in [0, 1), \quad (16)$$

which helps improve training stability. In practice, iterating over all elements in $\mathcal{G}_\mathcal{L}$ may be intractable. Thus, for each optimization step, $\mathcal{R}(\theta, \bar{\theta})$ is one-sample approximated by:

$$\mathcal{R}(\theta, \bar{\theta}) \approx \mathbb{E} \left[\|\mathbf{s}_\theta(A_h \mathbf{x}, t) - A_h \mathbf{s}_{\bar{\theta}}(\mathbf{x}, t)\|^2 \right], \quad (17)$$

with randomly picked $h \in \mathcal{G}_\mathcal{L}$.

5.2 $\mathcal{G}_\mathcal{L}$ -equivariant Trajectory Sampling

The sampling trajectory of the diffusion model is governed by the SDE in Eq (3), which can be written as

$$d\mathbf{x}_t = \bar{\mathbf{f}}_{\theta, \lambda}(\mathbf{x}_t, t) dt + \lambda g(t) dw_t \quad (18)$$

with $\bar{\mathbf{f}}_{\theta, \lambda}$ defined in Eq (11). In practice, the sampling process solves Eq (18) through Euler–Maruyama method:

$$\mathbf{x}_{i-1} \leftarrow \bar{\mathbf{f}}_{\theta, \lambda}(\mathbf{x}_i, t_i)(t_{i-1} - t_i) + \lambda g(t) \sqrt{t_i - t_{i-1}} \boldsymbol{\epsilon}_i \quad (19)$$

with preset time steps $\{t_i\}_{i=1}^n$ and $\boldsymbol{\epsilon}_i \sim \mathcal{N}(\mathbf{0}, I)$. It is desired in many industrial, and medical applications, that this sampling process is deterministic in which the output \mathbf{x}_0 barely depends on the starting point \mathbf{x}_n . This can be achieved by either setting $\lambda = 0$ or fixing the seed of the generator of $\boldsymbol{\epsilon}_i$ to obtain a deterministic noise sequence $\{\boldsymbol{\epsilon}_i\}_{i=1}^n$.

Under this setting, the trajectory is already equivariant for $\lambda = 0$ by applying the methods discussed in Sec 5.1 to make $\bar{\mathbf{f}}_{\theta, \lambda}$ equivariant. For $\lambda > 0$, we also need $\{\boldsymbol{\epsilon}_i\}_{i=1}^n$ to be “equivariant” such that for $h \in \mathcal{G}_\mathcal{L}$, if starting point \mathbf{x}_n is updated to $h(\mathbf{x}_n) = A_h \mathbf{x}_n$, the sequence $\{\boldsymbol{\epsilon}_i\}_{i=1}^n$ is also updated to $\{\tilde{\boldsymbol{\epsilon}}_i\}_{i=1}^n$ with $\tilde{\boldsymbol{\epsilon}}_i = A_h \boldsymbol{\epsilon}_i$.

To implement this without knowing the “true” orientation of \mathbf{x}_t , let q denote the distribution of \mathbf{x}_n . Construct a function $\phi : \mathbb{R}^d \rightarrow \mathbb{R}^d$ such that: (1) for all $h \in \mathcal{G}_\mathcal{L}$, $\mathbf{x} \sim q$ or $\mathbf{x} \sim \mathcal{N}(\mathbf{0}, I)$, $\phi(A_h \mathbf{x}) = A_h \phi(\mathbf{x})$ almost surely;

Table 2: Model summary. SPDdiff denotes the regular diffusion model. SPDdiff+Reg+OC combines the outputs of SPDdiff+Reg. ✓: Theo. guaranteed ✗: Not theo. guaranteed -: Not Applicable

Model	Arch.	$\mathcal{G}_{\mathcal{L}}$ -inv Smpl	Eqv Traj
SPDiff	U-Net	✗	✗
SPDiff+WT	U-Net (WT)	✓	✓
SPDiff+OC	U-Net	✓	✓
SPDiff+Reg	U-Net	✗	✗
SPDiff+Reg+OC	U-Net	✓	✓
SP-GAN	CNN	✓	-

(2) for all $\mathbf{x}, \mathbf{y} \in \mathbb{R}^d$, there exists a unique $\mathbf{h} \in \mathcal{G}_{\mathcal{L}}$ such that $\phi(\mathbf{x}) = A_{\mathbf{h}}\phi(\mathbf{y})$.⁴ Given starting point \mathbf{x}_n and a noisy sequence $\{\epsilon_i\}_{i=1}^n$, choose $\mathbf{h} \in \mathcal{G}_{\mathcal{L}}$ such that $\phi(\mathbf{x}_n) = A_{\mathbf{h}}\phi(\epsilon_n)$. Then we use the noisy sequence $\tilde{\epsilon}_i = A_{\mathbf{h}}\epsilon_i$ for the evaluation of Eq (19). To see why this approach works, assume \mathbf{x}_n is updated to $A_r\mathbf{x}_n$ for some $r \in \mathcal{G}_{\mathcal{L}}$. Then, $\phi(A_r\mathbf{x}_n) = A_r\phi(\mathbf{x}_n) = (A_rA_{\mathbf{h}})\phi(\epsilon_n)$, and thus the sequence becomes $\{A_rA_{\mathbf{h}}\epsilon_i\}_{i=1}^n = \{A_r\tilde{\epsilon}_i\}_{i=1}^n$. Note, this is a general method to create an equivariant noise sequence with respect to any input, which can also be used to inject equivariant noise into corrupted images as shown in Fig 1.

6 Empirical Study

In this section, we report a selection of experiments to demonstrate the effectiveness of the methods that we presented in Sec 5. The results corroborate our theoretical work discussed in Sec 4 and provide additional insights.

6.1 Datasets

Our study adopts two standard benchmark datasets, rotated MNIST Larochelle et al. 2007 and LYSTO Jiao et al. 2023, that are commonly used in the investigations of invariant generative models.

The rotated MNIST dataset, described in Larochelle et al. (2007), contains random 90 deg rotations of the MNIST images Deng 2012 resulting in an C_4 -invariant distribution. This dataset serves as a common evaluation benchmark for group invariant CNN-based models, being used in Dey et al. (2021) and Birrell et al. (2022) to measure the sensitivity of model performance to dataset size with models being trained on 1%(600), 5%(3000), and 10%(6000) of the dataset. All the models tested on this dataset assume C_4 invariance.

The LYSTO Jiao et al. 2023 dataset contains 20,000 image patches extracted from whole-slide images of breast, colon, and prostate cancer samples stained with one of CD3 or CD8 immunohistochemical marker dyes. This data exhibits natural rotational and mirror invariance as there is no one correct orientation of individual samples when used in medical screening. Moreover, these images possess highly structured features that should be faithfully replicated by any method that seeks to generate new samples based on this data, thus serving as a representative benchmark of model performance. All the models evaluated on the LYSTO dataset assume group D_4 invariance, meaning that the distribution remains unchanged under 90 deg rotations combined with flipping operations. Additionally, following a methodology introduced in SP-GAN Birrell et al. 2022, the models are trained using randomly selected 64x64x3 crops from the 20,000 reference images in the LYSTO dataset, which were initially scaled to 128x128x3.

⁴E.g., for \mathbb{R}^2 with $\mathcal{G}_{\mathcal{L}}$ consisting of the identity and element-swapping operator, ϕ can be the function that outputs one-hot vector indicating the max element of the input. We present some selections of ϕ for common $\mathcal{G}_{\mathcal{L}}$ in appx C.

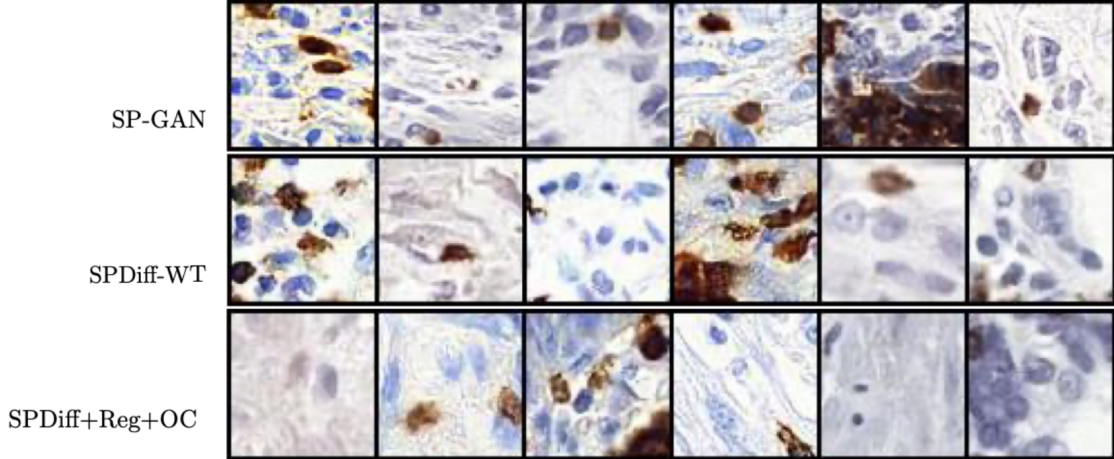


Figure 5: Images generated by the selected models trained on the LYSTO. Additional sample images are available in appx E.

6.2 Models

We implement diffusion models using VP-SDEs (Ho et al. 2020; Song et al. 2021a), which are structure-preserving, according to Cor 1, under C_4 and D_4 . Except for the model employing weight-tied CNN kernels (SPDiff-WT), all other models are trained using data samples augmented by randomly selected operators from their respective groups. As a baseline, we present the performance results for the standard diffusion model, SPDiff. We also report the performance of SP-GAN Birrell et al. 2022, the only GAN-based generative model that produces group invariant distribution with theoretical guarantees. We summarize the tested models with their invariance and equivariance properties in table 2.

To boost model performance, we follow the method in EDM Karras et al. 2022 to apply Non-leaky augmentation. The pipeline involves several geometric transformations applied to a training image before introducing noise. To prevent these augmentations from affecting the generated images, we include the augmentation parameters as a conditioning input to the network. During inference, we set them to zero to ensure that only non-augmented images are generated. Additionally, we apply self-conditioning Chen et al. 2023 to further improve the sample quality. Detailed model configurations can be found in appx D.

6.3 Results

We report the FID score Heusel et al. 2017 of the diffusion-based models and SP-GAN Birrell et al. 2022 in table 3 and table 4. To ensure consistency, we have reproduced the results of SP-GAN with necessary modifications based on the official code, enabling the computation of FID using the same code employed for our proposed models. For consistency, all scores are reported based on 50,000 randomly generated images. (Sample images of selected models are presented in Fig 5.) Across all datasets, it is evident that the diffusion-based models consistently outperform SP-GAN by a significant margin. Notably, SPDiff+WT, SPDiff+OC, and SPDiff+Reg+OC provide the same invariance guarantee.

Invariant sampling distribution. To measure the degree of \mathcal{G} -invariance of the sampling distribution, we propose a measure called *Inv-FID*. Given a set of generated images \mathcal{D}_s , Inv-FID returns the maximum FID between $h_1(\mathcal{D}_s)$ and $h_2(\mathcal{D}_s)$ for $h_1, h_2 \in \mathcal{G}$. If \mathcal{D}_s is perfectly \mathcal{G} -invariant, $h \in \mathcal{G}$ does not change the distribution of \mathcal{D}_s , and Inv-FID is zero; otherwise, the score is strictly greater than zero. From table 3 and 4, we observe that the diffusion models with theoretical guarantees indeed have lower scores, while the

Table 3: Model Comparison on 28x28x1 Rotated MNIST (Group C4). * indicates author-reported values.

Model	FID↓				Inv-FID↓	$\Delta\tilde{\mathbf{x}}_0$ ↓
	1%	5%	10%	100%	100%	100%
SPDiff	5.97	3.05	3.47	2.81	2.21	0.2997
SPDiff+WT	5.80	3.34	3.57	3.50	2.20	0.0004
SPDiff+OC	6.10	3.09	3.45	2.82	2.12	0.0002
SPDiff+Reg	5.42	3.69	2.83	2.75	2.09	0.1806
SPDiff+Reg+OC	5.64	3.67	2.86	2.64	2.07	0.0002
SP-GAN	149*	99*	88*	81*	–	–
SP-GAN (Reprod.)	16.59	11.28	9.02	10.95	19.92	–

Table 4: Model Comparison on LYSTO 64x64x3 image dataset (Group D_4). * indicates author-reported values.

Model	FID↓	Inv-FID ↓	$\Delta\tilde{\mathbf{x}}_0$ ↓
SPDiff	7.88	0.66	0.0845
SPDiff+WT (ours)	12.75	0.59	0.0002
SPDiff+OC (ours)	7.84	0.64	0.0001
SPDiff+Reg (ours)	6.66	0.60	0.0762
SPDiff+Reg+OC (ours)	6.64	0.60	$< 10^{-5}$
SP-GAN	205*	–	–
SP-GAN (Reprod.)	148.26	0.71	–

equivariance regularizer can also improve the invariance property. Furthermore, it’s worth noting that the differences in Inv-FID scores among the diffusion models are relatively small. This suggests that diffusion models have the capability to inherently learn the invariant properties, regardless of the specific techniques applied. Thus, in scenarios where sampling distribution invariance is not a critical requirement, regular diffusion models may suffice.

Validating equivariant sampling trajectory. To empirically show that our methods provide theoretical guarantees to obtain equivariant sampling trajectories, we test our methods by implementing an image-denoising task as demonstrated in Fig 1 using SDEdit Meng et al. 2022. Specifically, given a low-resolution (or corrupted) image $\tilde{\mathbf{x}}_0$, we add equivariant noise with respect to $\tilde{\mathbf{x}}_0$ through the technique discussed in Sec 5.2 to obtain \mathbf{x}_t . Then, we apply the same technique to inject noise when solving backward SDEs to obtain a denoised image $\text{dn}(\tilde{\mathbf{x}}_0)$ where dn represents the entire denoising process. As discussed in Sec 5.2, if a diffusion model is $\mathcal{G}_{\mathcal{L}}$ -equivariant guaranteed, we should have $\text{dn}(A_{\mathbf{h}}\tilde{\mathbf{x}}_0) - A_{\mathbf{h}}\text{dn}(\tilde{\mathbf{x}}_0) \approx \mathbf{0}$ for all $\mathbf{h} \in \mathcal{G}_{\mathcal{L}}$.

In table 3 and 4, we report the averaged maximum pixel-wise distance $\Delta\mathbf{x}_0$ between $\text{dn}(A_{\mathbf{h}}\tilde{\mathbf{x}}_0)$ and $A_{\mathbf{h}}\text{dn}(\tilde{\mathbf{x}}_0)$ over 16 randomly sampled corrupted $\tilde{\mathbf{x}}_0$ with 1/4 of the original resolution (and upsampled). \mathbf{h} is randomly picked for each $\tilde{\mathbf{x}}_0$. The result shows that the models that are theoretically equivariant consistently have nearly zero $\Delta\mathbf{x}_0$. In contrast, the models without theoretical guarantees will produce significantly different outputs, which could be problematic in some applications like medical image analysis.

How do our techniques affect sampling performance? Among the models that provide theoretical guarantees on the invariant sampling distribution and equivariant sampling trajectory, we notice that SPDiff+WT cannot achieve FID scores comparable to the output-combining methods on complicated datasets (e.g. LYSTO). This is probably because the weight-tying technique constrains the expressiveness of the model and makes it harder to optimize. In contrast, the output-combining method does not affect the model’s sample quality as the underlying neural network and the training process is unchanged.

Equivariance regularization improves sampling quality. We observe that by effectively enhancing the

equivariance property of the models, the regularizer $\mathcal{R}(\boldsymbol{\theta}, \bar{\boldsymbol{\theta}})$ in Eq (15) helps models learn and enhances their quality of sampling on nearly all datasets. We believe this happens because 1) the additional constraints alleviate the overfitting problem, and 2) the regularizer allows the model to improve the estimated score at one point using another estimator at an equivalent point. Specifically, as discussed in Sec 5.1 (above Eq (13)), $A_h^{-1} \mathbf{s}_\theta(A_h \mathbf{x}, t)$ are also valid estimators of score $\nabla_{\mathbf{x}} \log p_t(\mathbf{x})$ for $h \in \mathcal{G}_{\mathcal{L}}$. By matching these values with $\mathbf{s}_\theta(\mathbf{x}, t)$, $\mathcal{R}(\boldsymbol{\theta}, \bar{\boldsymbol{\theta}})$ guides the model to improve its estimation through the equivalent estimators.

7 Discussion

In this work we have demonstrated a way of effectively constraining diffusion models to obey group equivariant properties for use in learning \mathcal{G} -invariant probability distributions. The proposed methods were experimentally verified over a selection of both synthetic and real-world datasets, in which we achieved considerable gains in performance measured against existing equivariant models. We also established new theoretical guarantees for exactly when the diffusion process can be made equivariant w.r.t. a given group.

Acknowledgment

We gratefully acknowledge funding support from NSERC and the Canada CIFAR AI Chairs program. Resources used in preparing this research were provided, in part, by the Province of Ontario, the Government of Canada through CIFAR, and companies sponsoring the Vector Institute.

References

- Albergo, M. S., N. M. Boffi, and E. Vanden-Eijnden (2023). “Stochastic Interpolants: A Unifying Framework for Flows and Diffusions”. arXiv:2303.08797.
- Albergo, M. S. and E. Vanden-Eijnden (2023). “Building Normalizing Flows with Stochastic Interpolants”. In: *The Eleventh International Conference on Learning Representations*.
- Anderson, B. D. (1982). “Reverse-time diffusion equation models”. *Stochastic Processes and their Applications*, vol. 12, no. 3, pp. 313–326.
- Baranchuk, D., A. Voynov, I. Rubachev, V. Khruikov, and A. Babenko (2022). “Label-Efficient Semantic Segmentation with Diffusion Models”. In: *International Conference on Learning Representations*.
- Biloš, M. and S. Günnemann (July 2021). “Scalable Normalizing Flows for Permutation Invariant Densities”. In: *Proceedings of the 38th International Conference on Machine Learning*. Ed. by M. Meila and T. Zhang. Vol. 139. Proceedings of Machine Learning Research. PMLR, pp. 957–967.
- Birrell, J., M. Katsoulakis, L. Rey-Bellet, and W. Zhu (July 2022). “Structure-preserving GANs”. In: *Proceedings of the 39th International Conference on Machine Learning*. Ed. by K. Chaudhuri, S. Jegelka, L. Song, C. Szepesvari, G. Niu, and S. Sabato. Vol. 162. Proceedings of Machine Learning Research. PMLR, pp. 1982–2020.
- Chen, S., S. Chewi, J. Li, Y. Li, A. Salim, and A. Zhang (2023). “Sampling is as easy as learning the score: theory for diffusion models with minimal data assumptions”. In: *The Eleventh International Conference on Learning Representations*.
- Cohen, T. and M. Welling (2016). “Group Equivariant Convolutional Networks”. In: *Proceedings of The 33rd International Conference on Machine Learning*. Ed. by M. F. Balcan and K. Q. Weinberger. Vol. 48. Proceedings of Machine Learning Research, pp. 2990–2999.
- Deng, L. (2012). “The mnist database of handwritten digit images for machine learning research”. *IEEE Signal Processing Magazine*, vol. 29, no. 6, pp. 141–142.
- Dey, N., A. Chen, and S. Ghafurian (2021). “Group Equivariant Generative Adversarial Networks”. In: *International Conference on Learning Representations*.
- Esteves, C., C. Allen-Blanchette, A. Makadia, and K. Daniilidis (2018). “Learning $SO(3)$ Equivariant Representations with Spherical CNNs”. In: *ECCV*, pp. 54–70.
- Gao, L., Y. Du, H. Li, and G. Lin (2022). “RotEqNet: Rotation-equivariant network for fluid systems with symmetric high-order tensors”. *Journal of Computational Physics*, vol. 461, p. 111205.
- Goldman, L. W. (2007). “Principles of CT: radiation dose and image quality”. *Journal of Nuclear Medicine Technology*, vol. 35, no. 4, pp. 213–225.

- Goodfellow, I. (2016). “Neurips 2016 tutorial: Generative adversarial networks”. *arXiv preprint arXiv:1701.00160*.
- Goodfellow, I., J. Pouget-Abadie, M. Mirza, B. Xu, D. Warde-Farley, S. Ozair, A. Courville, and Y. Bengio (2014). “Generative Adversarial Nets”. In: *Advances in Neural Information Processing Systems*. Vol. 27. Curran Associates, Inc.
- Heusel, M., H. Ramsauer, T. Unterthiner, B. Nessler, and S. Hochreiter (2017). “GANs Trained by a Two Time-Scale Update Rule Converge to a Local Nash Equilibrium”. In: *Advances in Neural Information Processing Systems*. Ed. by I. Guyon, U. V. Luxburg, S. Bengio, H. Wallach, R. Fergus, S. Vishwanathan, and R. Garnett. Vol. 30. Curran Associates, Inc.
- Ho, J., A. Jain, and P. Abbeel (2020). “Denoising Diffusion Probabilistic Models”. In: *Advances in Neural Information Processing Systems*. Ed. by H. Larochelle, M. Ranzato, R. Hadsell, M. Balcan, and H. Lin. Vol. 33. Curran Associates, Inc., pp. 6840–6851.
- Hoogeboom, E., V. G. Satorras, C. Vignac, and M. Welling (2022). “Equivariant Diffusion for Molecule Generation in 3D”. In: *Proceedings of the 39th International Conference on Machine Learning*, pp. 8867–8887.
- Huda, W. (2002). “Dose and image quality in CT”. *Pediatric Radiology*, vol. 32, no. 10, pp. 709–713.
- Jiao, Y. et al. (2023). “LYSTO: The Lymphocyte Assessment Hackathon and Benchmark Dataset”. arXiv:2301.06304.
- Karras, T., M. Aittala, T. Aila, and S. Laine (2022). “Elucidating the design space of diffusion-based generative models”. In: *Advances in Neural Information Processing Systems*.
- Khrulkov, V., G. Ryzhakov, A. Chertkov, and I. Oseledets (2023). “Understanding DDPM Latent Codes Through Optimal Transport”. In: *The Eleventh International Conference on Learning Representations*.
- Kim, D., C.-H. Lai, W.-H. Liao, N. Murata, Y. Takida, T. Uesaka, Y. He, Y. Mitsufuji, and S. Ermon (2023). “Consistency Trajectory Models: Learning Probability Flow ODE Trajectory of Diffusion”. *arXiv preprint arXiv:2310.02279*.
- Kingma, D. P. and J. Ba (2015). “Adam: A Method for Stochastic Optimization”. In: *3rd International Conference on Learning Representations, ICLR 2015, San Diego, CA, USA, May 7-9, 2015, Conference Track Proceedings*. Ed. by Y. Bengio and Y. LeCun.
- Knigge, D. M., D. W. Romero, and E. J. Bekkers (2022). “Exploiting Redundancy: Separable Group Convolutional Networks on Lie Groups”. In: *Proceedings of the 39th International Conference on Machine Learning*. Ed. by K. Chaudhuri, S. Jegelka, L. Song, C. Szepesvari, G. Niu, and S. Sabato. Vol. 162. Proceedings of Machine Learning Research. PMLR, pp. 11359–11386.
- Köhler, J., L. Klein, and F. Noe (2019). “Equivariant flows: sampling configurations for multi-body systems with symmetric energies”. In: *2nd Workshop on Machine Learning and the Physical Sciences (NeurIPS)*.
- (July 2020). “Equivariant Flows: Exact Likelihood Generative Learning for Symmetric Densities”. In: *Proceedings of the 37th International Conference on Machine Learning*. Ed. by H. D. III and A. Singh. Vol. 119. Proceedings of Machine Learning Research. PMLR, pp. 5361–5370.
- Kondor, R. and S. Trivedi (2018). “On the Generalization of Equivariance and Convolution in Neural Networks to the Action of Compact Groups”. In: *Proceedings of the 35th International Conference on Machine Learning*.

- Kong, Z., W. Ping, J. Huang, K. Zhao, and B. Catanzaro (2021). “DiffWave: A Versatile Diffusion Model for Audio Synthesis”. In: *International Conference on Learning Representations*.
- Lafarge, M. W., E. J. Bekkers, J. P. Pluim, R. Duits, and M. Veta (2021). “Roto-translation equivariant convolutional networks: Application to histopathology image analysis”. *Medical Image Analysis*, vol. 68, p. 101849.
- Larochelle, H., D. Erhan, A. Courville, J. Bergstra, and Y. Bengio (2007). “An Empirical Evaluation of Deep Architectures on Problems with Many Factors of Variation”. In: *Proceedings of the 24th International Conference on Machine Learning*.
- Liu, J., A. Kumar, J. Ba, J. Kiros, and K. Swersky (2019). “Graph Normalizing Flows”. In: *Advances in Neural Information Processing Systems*. Ed. by H. Wallach, H. Larochelle, A. Beygelzimer, F. d’Alché-Buc, E. Fox, and R. Garnett. Vol. 32. Curran Associates, Inc.
- Meng, C., Y. He, Y. Song, J. Song, J. Wu, J.-Y. Zhu, and S. Ermon (2022). “SDEdit: Guided Image Synthesis and Editing with Stochastic Differential Equations”. In: *International Conference on Learning Representations*.
- Oksendal, B. (2003). “Stochastic differential equations: an introduction with applications”. Springer Science & Business Media.
- Ravanbakhsh, S., J. Schneider, and B. Póczos (2017). “Equivariance Through Parameter-Sharing”. In: *Proceedings of the 34th International Conference on Machine Learning*.
- Rezende, D. J., S. Racanière, I. Higgins, and P. Toth (2019). “Equivariant Hamiltonian Flows”. arXiv:1909.13739.
- Rombach, R., A. Blattmann, D. Lorenz, P. Esser, and B. Ommer (June 2022). “High-Resolution Image Synthesis With Latent Diffusion Models”. In: *Proceedings of the IEEE/CVF Conference on Computer Vision and Pattern Recognition (CVPR)*, pp. 10684–10695.
- Ronneberger, O., P. Fischer, and T. Brox (2015). “U-Net: Convolutional Networks for Biomedical Image Segmentation”. In: *Medical Image Computing and Computer-Assisted Intervention – MICCAI 2015*. Ed. by N. Navab, J. Hornegger, W. M. Wells, and A. F. Frangi. Cham: Springer International Publishing, pp. 234–241.
- Salimans, T., A. Karpathy, X. Chen, and D. P. Kingma (2017). “PixelCNN++: Improving the PixelCNN with Discretized Logistic Mixture Likelihood and Other Modifications”. In: *International Conference on Learning Representations*.
- Satorras, V. G., E. Hoogeboom, F. B. Fuchs, I. Posner, and M. Welling (2021). “E(n) Equivariant Normalizing Flows”. In: *Advances in Neural Information Processing Systems*. Ed. by A. Beygelzimer, Y. Dauphin, P. Liang, and J. W. Vaughan.
- Shao, H.-C., Y. Li, J. Wang, S. Jiang, and Y. Zhang (2023). “Real-time liver motion estimation via deep learning-based angle-agnostic X-ray imaging”. *Medical Physics*, vol. 50, no. 11, pp. 6649–6662.
- Shawe-Taylor, J. (1993). “Symmetries and discriminability in feedforward network architectures”. *IEEE Transactions on Neural Networks*, vol. 4, no. 5, pp. 816–826.
- Shi, C., S. Luo, M. Xu, and J. Tang (2021). “Learning Gradient Fields for Molecular Conformation Generation”. In: *International Conference on Machine Learning*.

- Siemund, R., A. Love, D. van Westen, L. Stenberg, C. Petersen, and I. Bjorkman-Burtscher (2012). “Radiation dose reduction in CT of the brain: can advanced noise filtering compensate for loss of image quality?” *Acta Radiologica*, vol. 53, no. 4, pp. 468–472.
- Song, J., C. Meng, and S. Ermon (2021a). “Denoising Diffusion Implicit Models”. In: *International Conference on Learning Representations*.
- Song, Y., P. Dhariwal, M. Chen, and I. Sutskever (2023). “Consistency Models”. In: *Proceedings of the 40th International Conference on Machine Learning*.
- Song, Y. and S. Ermon (2019). “Generative Modeling by Estimating Gradients of the Data Distribution”. In: *Advances in Neural Information Processing Systems*. Ed. by H. Wallach, H. Larochelle, A. Beygelzimer, F. d’Alché-Buc, E. Fox, and R. Garnett. Vol. 32. Curran Associates, Inc.
- Song, Y., J. Sohl-Dickstein, D. P. Kingma, A. Kumar, S. Ermon, and B. Poole (2021b). “Score-Based Generative Modeling through Stochastic Differential Equations”. In: *International Conference on Learning Representations*.
- Stewart, J., D. Clegg, and S. Watson (2021). “Multivariable calculus”. eng. Ninth edition. Australia: Cengage.
- Wolleb, J., R. Sandkühler, F. Bieder, P. Valmaggia, and P. C. Cattin (2022). “Diffusion Models for Implicit Image Segmentation Ensembles”. In: *Proceedings of The 5th International Conference on Medical Imaging with Deep Learning*. Ed. by E. Konukoglu, B. Menze, A. Venkataraman, C. Baumgartner, Q. Dou, and S. Albarqouni. Vol. 172. Proceedings of Machine Learning Research. PMLR, pp. 1336–1348.
- Xu, M., L. Yu, Y. Song, C. Shi, S. Ermon, and J. Tang (2022). “GeoDiff: A Geometric Diffusion Model for Molecular Conformation Generation”. In: *International Conference on Learning Representations*.
- Zhang, Q. and Y. Chen (2023). “Fast Sampling of Diffusion Models with Exponential Integrator”. In: *The Eleventh International Conference on Learning Representations*.

A Derivation Details of the Theoretical Results

In this appendix, we give the proof of our theoretical results. Given $\mathbf{x}_0 \sim p_0$, let p_t denote the marginal distribution of \mathbf{x}_t induced by the SDE Eq (1). Our discussion is conducted under the following assumptions:

Assumption 1

1. The drift function $\mathbf{f}(\mathbf{x}, t)$ has a continuous first-order partial derivative with respect to \mathbf{x} and $\nabla_{\mathbf{x}}\mathbf{f}(\mathbf{x}, t)$ is continuous in t . The diffusion coefficient $g(t)$ is continuous.
2. All the second partial derivatives of $p_t(\mathbf{x})$ with respect to \mathbf{x} exist and are continuous in \mathbf{x} and t .
3. $p_t(\mathbf{x}) > 0$ for all $\mathbf{x} \in \mathbb{R}^d$ and $t \geq 0$.
4. For all $\mathbf{h} \in \mathcal{G}_{\mathcal{L}}$, \mathbf{h} is a linear isometry such that for all $\mathbf{x}, \mathbf{y} \in \mathbb{R}^d$, $\|\mathbf{h}(\mathbf{x}) - \mathbf{h}(\mathbf{y})\|_2 = \|\mathbf{x} - \mathbf{y}\|_2$.

A.1 Some Fundamental Results in Multivariable Calculus

As our proof relies on the divergence theorem and surface integral in \mathbb{R}^d that are usually introduced based on differential forms, for completeness and a better understanding of our results, we briefly introduce them here using traditional multivariate calculus notations without mention of differential forms.

Theorem 1 (Divergence theorem, Stewart et al. 2021) *Let $\mathbf{h}(x_1, x_2, \dots, x_n) = (h_1, h_2, \dots, h_n)$ be a smooth vector field on $U \subset \mathbb{R}^n$ with $h_1, h_2, \dots, h_n : U \rightarrow \mathbb{R}$ smooth functions. Let $\alpha : C \rightarrow \mathbb{R}^n$ be a parametric $(n - 1)$ -dimensional space, whose image $\partial E = \alpha(C)$ is closed. Let $E \subseteq \mathbb{R}^d$ be the region consisting of the closed surface ∂E and its interior. Let \mathbf{n} be the normal vector to ∂E pointing outwards. Then*

$$\int_E \nabla \cdot \mathbf{h}(\mathbf{x}) \, d\mathbf{x} = \int_E \sum_{k=1}^d \frac{\partial h_k}{\partial x_k}(\mathbf{x}) \, d\mathbf{x} = \int_{\partial E} \mathbf{h} \cdot \mathbf{n} \, dS, \quad (20)$$

where both sides should be understood as multiple integrals over the corresponding regions.

For the surface integral in Eq (20), it can be evaluated in a way similar to the \mathbb{R}^3 case. Specifically, we need an operator \otimes , analogue to the cross product, that takes $\mathbf{u}_1, \mathbf{u}_2, \dots, \mathbf{u}_{d-1} \in \mathbb{R}^d$ and outputs a vector $\mathbf{v} \in \mathbb{R}^d$ perpendicular to them with the norm $\|\mathbf{v}\|$ to be the volume $\text{Vol}^{d-1}(\mathbf{u}_{1:d-1})$ of the parallelotope in \mathbb{R}^{d-1} with $\{\mathbf{u}_i\}_{i=1}^{d-1}$ for sides.⁵ Thus, we define $\otimes(\mathbf{u}_1, \mathbf{u}_2, \dots, \mathbf{u}_{d-1}) = [v_1, v_2, \dots, v_d]^\top$, where v_k is the multiplier of \hat{i}_k in

$$\det \begin{bmatrix} \hat{\mathbf{i}} & \mathbf{u}_1 & \mathbf{u}_2 & \cdots & \mathbf{u}_{d-1} \end{bmatrix}, \quad (21)$$

with $\hat{\mathbf{i}} = [\hat{i}_1, \hat{i}_2, \dots, \hat{i}_d]^\top$. To see why this definition is sufficient, note that for any $\mathbf{w} \in \mathbb{R}^d$, we have

$$\mathbf{w} \cdot \otimes(\mathbf{u}_1, \mathbf{u}_2, \dots, \mathbf{u}_{d-1}) = \det [\mathbf{w}, \mathbf{u}_1, \mathbf{u}_2, \dots, \mathbf{u}_{d-1}]. \quad (22)$$

Hence, $\mathbf{u}_k \cdot \otimes(\mathbf{u}_1, \mathbf{u}_2, \dots, \mathbf{u}_{d-1}) = 0$ for all k , which implies \mathbf{u}_k is orthogonal to $\otimes(\mathbf{u}_1, \mathbf{u}_2, \dots, \mathbf{u}_{d-1})$. Besides, we note that the volume of the parallelotope in \mathbb{R}^d with $\{\mathbf{z}_i\}_{i=1}^d$ for sides is defined to be $\text{Vol}^d(\mathbf{z}_{1:d}) = |\det [\mathbf{z}_1, \mathbf{z}_2, \dots, \mathbf{z}_d]|$. As a result, the volume of the parallelotope in \mathbb{R}^d with sides $\otimes(\mathbf{u}_1, \mathbf{u}_2, \dots, \mathbf{u}_{d-1})$ and $\mathbf{u}_1, \mathbf{u}_2, \dots, \mathbf{u}_{d-1}$ can written in two ways:

$$\text{Vol}^d(\mathbf{u}_{d-1}, \otimes(\mathbf{u}_1, \mathbf{u}_2, \dots), \mathbf{u}_{1:d-1}) = \text{Vol}^{d-1}(\mathbf{u}_{1:d-1}) \cdot \|\otimes(\mathbf{u}_{1:d-1})\| \quad (23)$$

⁵Note that \otimes reduces to the regular cross product for $d = 3$.

or

$$\text{Vol}^d(\mathbf{u}_{d-1}, \otimes(\mathbf{u}_1, \mathbf{u}_2, \dots), \mathbf{u}_{1:d-1}) = |\det [\otimes(\mathbf{u}_{1:d-1}), \mathbf{u}_{1:d-1}]| = |\otimes(\mathbf{u}_{1:d-1}) \cdot \otimes(\mathbf{u}_{1:d-1})| = \|\otimes(\mathbf{u}_{1:d-1})\|^2. \quad (24)$$

Hence, the equality yields $\|\otimes(\mathbf{u}_{1:d-1})\|^2 = \text{Vol}^{d-1}(\mathbf{u}_{1:d-1}) \cdot \|\otimes(\mathbf{u}_{1:d-1})\|$. Namely,

$$\|\otimes(\mathbf{u}_{1:d-1})\| = \text{Vol}^{d-1}(\mathbf{u}_{1:d-1}), \quad (25)$$

as we required. Then given a parametrization $\alpha : C \subseteq \mathbb{R}^{d-1} \rightarrow \mathbb{R}^d$ of ∂E , the surface integral can be evaluated by

$$\int_{\partial E} \mathbf{h} \cdot \mathbf{n} \, d\mathcal{S} = \pm \int_C \mathbf{h}(\alpha(\mathbf{y})) \cdot \otimes \left(\frac{\partial \alpha(\mathbf{y})}{\partial y_1}, \frac{\partial \alpha(\mathbf{y})}{\partial y_2}, \dots, \frac{\partial \alpha(\mathbf{y})}{\partial y_{d-1}} \right) \, d\mathbf{y}, \quad (26)$$

where the sign depends on the orientation of $\otimes \left(\frac{\partial \alpha(\mathbf{y})}{\partial y_1}, \frac{\partial \alpha(\mathbf{y})}{\partial y_2}, \dots, \frac{\partial \alpha(\mathbf{y})}{\partial y_{d-1}} \right)$.

We then discuss some change-of-variable properties of \otimes , which are summarized in the following lemmas for later reference.

Lemma 2 For an invertible matrix $M \in \mathbb{R}^{(d-1) \times (d-1)}$ and vectors $\mathbf{a}_1, \mathbf{a}_2, \dots, \mathbf{a}_{d-1} \in \mathbb{R}^d$, we have

$$\otimes(M\mathbf{a}_1, M\mathbf{a}_2, \dots, M\mathbf{a}_{d-1}) = (\det M) (M^{-1})^\top \otimes(\mathbf{a}_1, \mathbf{a}_2, \dots, \mathbf{a}_{d-1}). \quad (27)$$

Proof: Let \mathbf{e}_i denote the one-hot vector with its i -th entry equal to one. Then by Eq (22), we have for all $i = 1, 2, \dots, d$,

$$\mathbf{e}_i \cdot \otimes(M\mathbf{a}_1, M\mathbf{a}_2, \dots, M\mathbf{a}_{d-1}) \quad (28)$$

$$= \det [\mathbf{e}_i, M\mathbf{a}_1, M\mathbf{a}_2, \dots, M\mathbf{a}_{d-1}] = \det \left(M [M^{-1}\mathbf{e}_i, \mathbf{a}_1, \mathbf{a}_2, \dots, \mathbf{a}_{d-1}] \right) \quad (29)$$

$$= \det M \cdot \det [M^{-1}\mathbf{e}_i, \mathbf{a}_1, \mathbf{a}_2, \dots, \mathbf{a}_{d-1}] = \det M \cdot \left\{ M^{-1}\mathbf{e}_i \cdot \otimes(\mathbf{a}_1, \mathbf{a}_2, \dots, \mathbf{a}_{d-1}) \right\} \quad (30)$$

$$= \det M \cdot \left\{ \mathbf{e}_i^\top (M^{-1})^\top \otimes(\mathbf{a}_1, \mathbf{a}_2, \dots, \mathbf{a}_{d-1}) \right\}. \quad (31)$$

Then, aggregately, we have Eq (27). ■

Lemma 3 Let $\mathbf{h} : \mathbb{R}^d \rightarrow \mathbb{R}^d$ be a continuously differential function with $|\det D\mathbf{h}(\mathbf{x})| = 1$ for all $\mathbf{x} \in \mathbb{R}^d$ and $\boldsymbol{\eta} : \mathbb{R}^d \rightarrow \mathbb{R}^d$ a continuous function. Then, for a closed and bounded set E , we have

$$\int_{\partial \mathbf{h}(E)} \boldsymbol{\eta} \cdot \mathbf{n} \, d\mathcal{S} = \int_{\partial E} (D\mathbf{h}(\mathbf{x}))^{-1} \boldsymbol{\eta}(\mathbf{h}(\mathbf{x})) \cdot \mathbf{n}(\mathbf{x}) \, d\mathcal{S}. \quad (32)$$

Proof: Let $\alpha : C \subseteq \mathbb{R}^{d-1} \rightarrow \mathbb{R}^d$ be a parametrization of ∂E . Then $\mathbf{h} \circ \alpha$ is a parametrization of $\partial \mathbf{h}(E)$. So we have

$$\int_{\partial \mathbf{h}(E)} \boldsymbol{\eta} \cdot \mathbf{n} \, d\mathcal{S} = \int_C \boldsymbol{\eta}(\mathbf{h} \circ \alpha(\mathbf{y})) \cdot \otimes \left(\frac{\partial \mathbf{h} \circ \alpha(\mathbf{y})}{\partial y_1}, \frac{\partial \mathbf{h} \circ \alpha(\mathbf{y})}{\partial y_2}, \dots, \frac{\partial \mathbf{h} \circ \alpha(\mathbf{y})}{\partial y_{d-1}} \right) \, d\mathbf{y}. \quad (33)$$

As $\frac{\partial \mathbf{h} \circ \alpha(\mathbf{y})}{\partial y_i} = D\mathbf{h}(\alpha(\mathbf{y})) \frac{\partial \alpha(\mathbf{y})}{\partial y_i}$, by Lem 2 with $M = D\mathbf{h}(\alpha(\mathbf{y}))$, we have

$$\boldsymbol{\eta}(\mathbf{h} \circ \alpha(\mathbf{y})) \cdot \otimes \left(\frac{\partial \mathbf{h} \circ \alpha(\mathbf{y})}{\partial y_1}, \frac{\partial \mathbf{h} \circ \alpha(\mathbf{y})}{\partial y_2}, \dots, \frac{\partial \mathbf{h} \circ \alpha(\mathbf{y})}{\partial y_{d-1}} \right) \quad (34)$$

$$= \left(((D\mathbf{h}(\alpha(\mathbf{y})))^{-1})^\top \boldsymbol{\eta}(\mathbf{h} \circ \alpha(\mathbf{y})) \right) \cdot \otimes \left(\frac{\partial \alpha(\mathbf{y})}{\partial y_1}, \frac{\partial \alpha(\mathbf{y})}{\partial y_2}, \dots, \frac{\partial \alpha(\mathbf{y})}{\partial y_{d-1}} \right). \quad (35)$$

Therefore,

$$\int_{\partial h(E)} \boldsymbol{\eta} \cdot \mathbf{n} \, d\mathcal{S} = \int_C \left(((Dh(\alpha(\mathbf{y})))^{-1})^\top \boldsymbol{\eta}(h \circ \alpha(\mathbf{y})) \right) \cdot \otimes \left(\frac{\partial \alpha(\mathbf{y})}{\partial y_1}, \frac{\partial \alpha(\mathbf{y})}{\partial y_2}, \dots, \frac{\partial \alpha(\mathbf{y})}{\partial y_{d-1}} \right) \, d\mathbf{y} \quad (36)$$

$$= \int_{\partial E} (Dh(\mathbf{x}))^{-1} \boldsymbol{\eta}(h(\mathbf{x})) \cdot \mathbf{n}(\mathbf{x}) \, d\mathcal{S}. \quad (37)$$

■

A.2 Some Fundamental Results About Linear Isometry

Lemma 4 *Let h be a linear isometry. Then its Jacobian Dh satisfies $|\det Dh| = 1$ and $(Dh)^\top (Dh) = I$.*

Proof: Since h is a linear isometry, we can write $h(\mathbf{x}) = A_h \mathbf{x}$ for some $A_h \in \mathbb{R}^d$. And the Jacobian $Dh = A_h$. According to the definition, for all $\mathbf{x}, \mathbf{y} \in \mathbb{R}^d$, we have $\|h(\mathbf{x}) - h(\mathbf{y})\|_2 = \|\mathbf{x} - \mathbf{y}\|_2$, which implies $\|A_h(\mathbf{x} - \mathbf{y})\|_2^2 = \|\mathbf{x} - \mathbf{y}\|_2^2$ and thus the matrix norm $\|A_h\| = 1$. Therefore, we have

$$\|\mathbf{x} - \mathbf{y}\|_2^2 = \|A_h(\mathbf{x} - \mathbf{y})\|_2^2 = \langle A_h^\top A_h(\mathbf{x} - \mathbf{y}), \mathbf{x} - \mathbf{y} \rangle \leq \|A_h^\top A_h(\mathbf{x} - \mathbf{y})\|_2 \|\mathbf{x} - \mathbf{y}\|_2. \quad (38)$$

For the last term,

$$\|A_h^\top A_h(\mathbf{x} - \mathbf{y})\|_2 \|\mathbf{x} - \mathbf{y}\|_2 \leq \|A_h^\top\| \|A_h\| \|\mathbf{x} - \mathbf{y}\|_2 \leq \|\mathbf{x} - \mathbf{y}\|_2^2. \quad (39)$$

As a result, we have

$$\|\mathbf{x} - \mathbf{y}\|_2^2 = \|A_h(\mathbf{x} - \mathbf{y})\|_2^2 = \langle A_h^\top A_h(\mathbf{x} - \mathbf{y}), \mathbf{x} - \mathbf{y} \rangle \leq \|A_h^\top A_h(\mathbf{x} - \mathbf{y})\|_2 \|\mathbf{x} - \mathbf{y}\|_2 \leq \|\mathbf{x} - \mathbf{y}\|_2^2. \quad (40)$$

Since we start and end with $\|\mathbf{x} - \mathbf{y}\|_2^2$, the equality holds everywhere including the Cauchy-Schwarz inequality in the middle. Note that the Cauchy-Schwarz inequality becomes equality only when $A_h^\top A_h(\mathbf{x} - \mathbf{y})$ is a scalar multiple of $\mathbf{x} - \mathbf{y}$, and this multiple has to be one to make the last inequality equal. As a result, we have $A_h^\top A_h(\mathbf{x} - \mathbf{y}) = \mathbf{x} - \mathbf{y}$ for all $\mathbf{x} - \mathbf{y}$. Hence, $A_h^\top A_h = I$ and $(\det A_h)^2 = 1$, which completes the proof. ■

Corollary 2 *If h is a linear isometry, we have $Dh(x)^\top = Dh(x)^{-1}$.*

Proof: This is due to the fact that $Dh(x)$ is orthonormal by Lem 4. ■

A.3 Properties of Structure-preserving Diffusion Models

Lemma 5 *Let p_t be the marginal distribution of \mathbf{x}_t satisfying SDE Eq (1). Then, the ODE*

$$d\mathbf{x} = \tilde{\mathbf{f}}(\mathbf{x}, t) \, dt \quad (41)$$

with

$$\tilde{\mathbf{f}}(\mathbf{x}, t) = \mathbf{f}(\mathbf{x}, t) - \frac{1}{2} g(t)^2 \nabla \log p_t(\mathbf{x}) \quad (42)$$

also has the same marginal distribution p_t for all $t \geq 0$.

Proof: The marginal distribution $p_t(\mathbf{x})$ evolution is characterized by the Fokker-Planck equation (Oksendal 2003):

$$\frac{\partial p_t(\mathbf{x})}{\partial t} = -\nabla \cdot (\mathbf{f}(\mathbf{x}, t)p_t(\mathbf{x})) + \frac{1}{2}\nabla \cdot \nabla (g(t)^2 p_t(\mathbf{x})) \quad (43)$$

$$= -\sum_{i=1}^d \frac{\partial}{\partial x_i} [f_i(\mathbf{x}, t)p_t(\mathbf{x})] + \frac{1}{2}\sum_{i=1}^d \frac{\partial^2}{\partial x_i^2} [g(t)^2 p_t(\mathbf{x})]. \quad (44)$$

That is,

$$\frac{\partial p_t(\mathbf{x})}{\partial t} = -\sum_{i=1}^d \left\{ \frac{\partial}{\partial x_i} [f_i(\mathbf{x}, t)p_t(\mathbf{x})] - \frac{\partial}{\partial x_i} \left[\frac{g(t)^2}{2} \frac{\partial}{\partial x_i} p_t(\mathbf{x}) \right] \right\} \quad (45)$$

$$= -\sum_{i=1}^d \frac{\partial}{\partial x_i} \left\{ [f_i(\mathbf{x}, t)p_t(\mathbf{x})] - \frac{g(t)^2}{2} [p_t(\mathbf{x}) \frac{\partial}{\partial x_i} \log p_t(\mathbf{x})] \right\} \quad (46)$$

$$= -\sum_{i=1}^d \frac{\partial}{\partial x_i} \left[f_i(\mathbf{x}, t) - \frac{g(t)^2}{2} \frac{\partial}{\partial x_i} \log p_t(\mathbf{x}) \right] p_t(\mathbf{x}), \quad (47)$$

which is the Fokker-Planck equation of

$$d\mathbf{x} = \tilde{\mathbf{f}}(\mathbf{x}, t) dt \quad (48)$$

with $\tilde{\mathbf{f}}(\mathbf{x}, t)$ given in Eq (42). ■

Lemma 6 $p(\mathbf{x})$ is \mathcal{G} -invariant if and only if $p(\mathbf{h}(\mathbf{x})) = p(\mathbf{x})$ for all $\mathbf{h} \in \mathcal{G}$ and $\mathbf{x} \in \mathbb{R}^d$.

Proof: Note that p is \mathcal{G} -invariant if and only if for any $\mathbf{h} \in \mathcal{G}$ and closed ball $B \subseteq \mathbb{R}^d$, $\int_B p(\mathbf{x}) d\mathbf{x} = \int_{\mathbf{h}(B)} p(\mathbf{h}(\mathbf{x})) d\mathbf{x}$. That is, $\int_B p(\mathbf{x}) d\mathbf{x} = \int_{\mathbf{h}(B)} p(\mathbf{x}) d\mathbf{x} = \int_B p(\mathbf{x}) |\det Dh| d\mathbf{x}$. As the equality holds for all B and $|\det Dh|$ is assumed to be one, $p(\mathbf{x}) = p(\mathbf{h}(\mathbf{x})) |\det Dh| = p(\mathbf{h}(\mathbf{x}))$ for all $\mathbf{x} \in \mathbb{R}^d$. Since every step is reversible, the proof is completed. ■

Lemma 1 $p(\mathbf{x})$ is $\mathcal{G}_{\mathcal{L}}$ -invariant if and only if

$$\mathbf{s}(\mathbf{h}(\mathbf{x})) = Dh(\mathbf{x}) \mathbf{s}(\mathbf{x}) \quad (7)$$

for all $\mathbf{h} \in \mathcal{G}_{\mathcal{L}}$ and $\mathbf{x} \in \mathbb{R}^d$, where $\mathbf{s}(\mathbf{x})$ denotes the score function $\nabla_{\mathbf{x}} \log p(\mathbf{x})$ and Dh the Jacobian matrix of \mathbf{h} .

Proof: (\Rightarrow) By Lem 6, if $p(\mathbf{x})$ is \mathcal{G} -invariant, $p(\mathbf{x}) = p(\mathbf{h}(\mathbf{x}))$. Taking log on both sides, followed by taking the derivative with respect to \mathbf{x} yields

$$\mathbf{s}(\mathbf{x}) = (Dh(\mathbf{x}))^{\top} \mathbf{s}(\mathbf{h}(\mathbf{x})). \quad (49)$$

Since \mathbf{h} is assumed to be a linear isometry, by Cor 2, $(Dh(\mathbf{x}))^{\top} = (Dh(\mathbf{x}))^{-1}$. Therefore, $\mathbf{s}(\mathbf{x}) = (Dh(\mathbf{x}))^{-1} \mathbf{s}(\mathbf{h}(\mathbf{x}))$ which is Eq (7).

(\Leftarrow) Given $\mathbf{s}(\mathbf{h}(\mathbf{x})) = Dh(\mathbf{x}) \mathbf{s}(\mathbf{x})$ for all $\mathbf{x} \in \mathbb{R}^d$ and $\mathbf{h} \in \mathcal{G}$, we have $\mathbf{s}(\mathbf{x}) = Dh(\mathbf{x})^{\top} \mathbf{s}(\mathbf{h}(\mathbf{x}))$. Therefore, we also have $\log p(\mathbf{x}) = \log p(\mathbf{h}(\mathbf{x})) + c$ for some constant c . That is, $p(\mathbf{x}) = p(\mathbf{h}(\mathbf{x})) \exp(c)$. As the integration with respect to \mathbf{x} over \mathbb{R}^d on both sides is one, $\exp(c) = 1$ and thus $p(\mathbf{x}) = p(\mathbf{h}(\mathbf{x}))$. Applying Lem 6 completes the proof. ■

Proposition 1 Let $\mathcal{G}_{\mathcal{L}}$ be a group comprised of linear isometries on \mathbb{R}^d . Consider a diffusion process taking the form in Eq (1) with $\mathcal{G}_{\mathcal{L}}$ -invariant p_0 . Then, p_t is $\mathcal{G}_{\mathcal{L}}$ -invariant for all $t \geq 0$ if and only if

$$Dh(\mathbf{x}) \mathbf{f}(\mathbf{x}, t) = \mathbf{f}(h(\mathbf{x}), t) \quad (9)$$

for all $t \geq 0$, $\mathbf{x} \in \mathbb{R}^d$ and $h \in \mathcal{G}_{\mathcal{L}}$.

Proof: (\Rightarrow) Assume that p_t is $\mathcal{G}_{\mathcal{L}}$ -invariant for all $t \geq 0$. Then, by Lem 5, we know that the forward process can be equivalently written as

$$d\mathbf{x} = \tilde{\mathbf{f}}(\mathbf{x}, t) dt \quad (50)$$

with $\tilde{\mathbf{f}}(\mathbf{x}, t) = \mathbf{f}(\mathbf{x}, t) - \frac{1}{2}g(t)^2 \nabla \log p_t(\mathbf{x})$. We first show that

$$Dh(\mathbf{x}) \tilde{\mathbf{f}}(\mathbf{x}, t) = \tilde{\mathbf{f}}(h(\mathbf{x}), t), \quad (51)$$

for all $h \in \mathcal{G}_{\mathcal{L}}$ and $\mathbf{x} \in \mathbb{R}^d$.

As p_t is $\mathcal{G}_{\mathcal{L}}$ -invariant for all $t \geq 0$, by Lem 6, $p_t(h(\mathbf{x})) = p_t(\mathbf{x})$ for all t . Thus, for any closed ball $\mathcal{A} \in \mathbb{R}^d$, we have

$$\int_{\mathcal{A}} \left[p_0(\mathbf{x}) + \int_0^t \frac{\partial}{\partial s} p_s(\mathbf{x}) ds \right] d\mathbf{x} = \int_{\mathcal{A}} p_t(\mathbf{x}) d\mathbf{x} = \int_{h(\mathcal{A})} p_t(\mathbf{y}) d\mathbf{y} = \int_{h(\mathcal{A})} \left[p_0(\mathbf{y}) + \int_0^t \frac{\partial}{\partial s} p_s(\mathbf{y}) ds \right] d\mathbf{x}. \quad (52)$$

Additionally, due to the $\mathcal{G}_{\mathcal{L}}$ -invariance of p_0 , we also have

$$\int_{\mathcal{A}} p_0(\mathbf{x}) d\mathbf{x} = \int_{h(\mathcal{A})} p_0(\mathbf{y}) d\mathbf{y}. \quad (53)$$

As a result,

$$\int_{\mathcal{A}} \int_0^t \frac{\partial}{\partial s} p_s(\mathbf{x}) ds d\mathbf{x} = \int_{h(\mathcal{A})} \int_0^t \frac{\partial}{\partial s} p_s(\mathbf{y}) ds d\mathbf{y}. \quad (54)$$

By the Fokker-Planck equation (Oksendal 2003), we have

$$\frac{\partial}{\partial t} p_t(\mathbf{x}) = - \sum_{i=1}^d \frac{\partial}{\partial x_i} (\tilde{f}_i(\mathbf{x}) p_t(\mathbf{x})) \quad \text{and} \quad \frac{\partial}{\partial t} p_t(h(\mathbf{x})) = - \sum_{i=1}^d \left[\frac{\partial}{\partial y_i} (\tilde{f}_i(\mathbf{y}) p_t(\mathbf{y})) \right]_{\mathbf{y}=h(\mathbf{x})} \quad \text{for all } h \in \mathcal{G}_{\mathcal{L}}. \quad (55)$$

Thus, Eq (54) becomes

$$\int_{\mathcal{A}} \int_0^t \sum_{i=1}^d \frac{\partial}{\partial x_i} (\tilde{f}_i(\mathbf{x}) p_t(\mathbf{x})) ds d\mathbf{x} = \int_{h(\mathcal{A})} \int_0^t \sum_{i=1}^d \frac{\partial}{\partial y_i} (\tilde{f}_i(\mathbf{y}) p_t(\mathbf{y})) ds d\mathbf{y}. \quad (56)$$

Or equivalently,

$$\int_0^t \int_{\mathcal{A}} \sum_{i=1}^d \frac{\partial}{\partial x_i} (\tilde{f}_i(\mathbf{x}) p_t(\mathbf{x})) d\mathbf{x} ds = \int_0^t \int_{h(\mathcal{A})} \sum_{i=1}^d \frac{\partial}{\partial y_i} (\tilde{f}_i(\mathbf{y}) p_t(\mathbf{y})) d\mathbf{y} ds. \quad (57)$$

Applying theorem 1, we can rewrite the integrals of the divergence of $\tilde{\mathbf{f}}(\mathbf{x}) p_t(\mathbf{x})$ over \mathcal{A} and $h(\mathcal{A})$ as surface integrals

$$\int_0^t \left[\int_{\partial \mathcal{A}} (\tilde{\mathbf{f}}(\mathbf{x}) p_t(\mathbf{x})) \cdot \mathbf{n} d\mathcal{S} \right] ds = \int_0^t \left[\int_{\partial h(\mathcal{A})} (\tilde{\mathbf{f}}(\mathbf{y}) p_t(\mathbf{y})) \cdot \mathbf{n} d\mathcal{S} \right] ds. \quad (58)$$

Thus,

$$\int_{\partial\mathcal{A}} (\tilde{\mathbf{f}}(\mathbf{x})p_t(\mathbf{x})) \cdot \mathbf{n} \, d\mathcal{S} = \int_{\partial\mathbf{h}(\mathcal{A})} (\tilde{\mathbf{f}}(\mathbf{y})p_t(\mathbf{y})) \cdot \mathbf{n} \, d\mathcal{S}. \quad (59)$$

Let $\alpha_{\mathcal{A}} : \mathbb{R}^{d-1} \rightarrow \mathbb{R}^d$ be a parametrization of surface $\partial\mathcal{A}$, and thus $\mathbf{h} \circ \alpha_{\mathcal{A}}$ is a parametrization of surface $\partial\mathbf{h}(\mathcal{A})$. Then Eq (59) can be written as

$$\pm \int_{\mathbb{R}^{d-1}} [\tilde{\mathbf{f}}(\alpha_{\mathcal{A}}(\mathbf{u}))p_t(\alpha_{\mathcal{A}}(\mathbf{u}))] \cdot \otimes \left(\frac{\partial\alpha_{\mathcal{A}}}{\partial u_1}, \frac{\partial\alpha_{\mathcal{A}}}{\partial u_2}, \dots, \frac{\partial\alpha_{\mathcal{A}}}{\partial u_{d-1}} \right) \, d\mathbf{u} \quad (60)$$

$$= \pm \text{sign}(\mathbf{h}) \int_{\mathbb{R}^{d-1}} [\tilde{\mathbf{f}}(\mathbf{h} \circ \alpha_{\mathcal{A}}(\mathbf{u}))p_t(\mathbf{h} \circ \alpha_{\mathcal{A}}(\mathbf{u}))] \cdot \otimes \left(\frac{\partial\mathbf{h} \circ \alpha_{\mathcal{A}}}{\partial u_1}, \frac{\partial\mathbf{h} \circ \alpha_{\mathcal{A}}}{\partial u_2}, \dots, \frac{\partial\mathbf{h} \circ \alpha_{\mathcal{A}}}{\partial u_{d-1}} \right) \, d\mathbf{u} \quad (61)$$

where $\text{sign}(\mathbf{h}) = \text{sign}(\det D\mathbf{h})$ that equals 1 if $\det D\mathbf{h} > 0$ and -1 otherwise.⁶

Hence, we have

$$[\tilde{\mathbf{f}}(\alpha_{\mathcal{A}}(\mathbf{u}))p_t(\alpha_{\mathcal{A}}(\mathbf{u}))] \cdot \otimes \left(\frac{\partial\alpha_{\mathcal{A}}}{\partial u_1}, \frac{\partial\alpha_{\mathcal{A}}}{\partial u_2}, \dots, \frac{\partial\alpha_{\mathcal{A}}}{\partial u_{d-1}} \right) \quad (62)$$

$$= \text{sign}(\mathbf{h}) [\tilde{\mathbf{f}}(\mathbf{h} \circ \alpha_{\mathcal{A}}(\mathbf{u}))p_t(\mathbf{h} \circ \alpha_{\mathcal{A}}(\mathbf{u}))] \cdot \otimes \left(\frac{\partial\mathbf{h} \circ \alpha_{\mathcal{A}}}{\partial u_1}, \frac{\partial\mathbf{h} \circ \alpha_{\mathcal{A}}}{\partial u_2}, \dots, \frac{\partial\mathbf{h} \circ \alpha_{\mathcal{A}}}{\partial u_{d-1}} \right) \quad (63)$$

Note that, by Lem 2,

$$\otimes \left(\frac{\partial\mathbf{h} \circ \alpha_{\mathcal{A}}}{\partial u_1}, \frac{\partial\mathbf{h} \circ \alpha_{\mathcal{A}}}{\partial u_2}, \dots, \frac{\partial\mathbf{h} \circ \alpha_{\mathcal{A}}}{\partial u_{d-1}} \right) = \det(D\mathbf{h}(\alpha_{\mathcal{A}}(\mathbf{u}))) \left((D\mathbf{h}(\mathbf{u}))^{-1} \right)^T \otimes \left(\frac{\partial\alpha_{\mathcal{A}}}{\partial u_1}, \frac{\partial\alpha_{\mathcal{A}}}{\partial u_2}, \dots, \frac{\partial\alpha_{\mathcal{A}}}{\partial u_{d-1}} \right), \quad (64)$$

and by the invariance of p_t

$$p_t(\mathbf{h} \circ \alpha_{\mathcal{A}}(\mathbf{u})) = p_t(\alpha_{\mathcal{A}}(\mathbf{u})). \quad (65)$$

Therefore, Eq (63) is equivalent to

$$[\tilde{\mathbf{f}}(\alpha_{\mathcal{A}}(\mathbf{u}))p_t(\mathbf{h} \circ \alpha_{\mathcal{A}}(\mathbf{u}))] \cdot \otimes \left(\frac{\partial\alpha_{\mathcal{A}}}{\partial u_1}, \frac{\partial\alpha_{\mathcal{A}}}{\partial u_2}, \dots, \frac{\partial\alpha_{\mathcal{A}}}{\partial u_{d-1}} \right) \quad (66)$$

$$= \left| \det(D\mathbf{h}(\alpha_{\mathcal{A}}(\mathbf{u}))) \right| [\tilde{\mathbf{f}}(\mathbf{h} \circ \alpha_{\mathcal{A}}(\mathbf{u}))p_t(\mathbf{h} \circ \alpha_{\mathcal{A}}(\mathbf{u}))] \cdot \left\{ \left((D\mathbf{h}(\mathbf{u}))^{-1} \right)^T \otimes \left(\frac{\partial\alpha_{\mathcal{A}}}{\partial u_1}, \frac{\partial\alpha_{\mathcal{A}}}{\partial u_2}, \dots, \frac{\partial\alpha_{\mathcal{A}}}{\partial u_{d-1}} \right) \right\} \quad (67)$$

$$= [\tilde{\mathbf{f}}(\mathbf{h} \circ \alpha_{\mathcal{A}}(\mathbf{u}))p_t(\mathbf{h} \circ \alpha_{\mathcal{A}}(\mathbf{u}))] \cdot \left\{ \left((D\mathbf{h}(\mathbf{u}))^{-1} \right)^T \otimes \left(\frac{\partial\alpha_{\mathcal{A}}}{\partial u_1}, \frac{\partial\alpha_{\mathcal{A}}}{\partial u_2}, \dots, \frac{\partial\alpha_{\mathcal{A}}}{\partial u_{d-1}} \right) \right\}, \quad (68)$$

$$(69)$$

where the last equality is due to the fact that \mathbf{h} is a linear isometry and Lem 4.

Rearranging Eq (68) yields

$$[\tilde{\mathbf{f}}(\alpha_{\mathcal{A}}(\mathbf{u}))p_t(\mathbf{h} \circ \alpha_{\mathcal{A}}(\mathbf{u}))] \cdot \otimes \left(\frac{\partial\alpha_{\mathcal{A}}}{\partial u_1}, \frac{\partial\alpha_{\mathcal{A}}}{\partial u_2}, \dots, \frac{\partial\alpha_{\mathcal{A}}}{\partial u_{d-1}} \right) \quad (70)$$

$$= [\tilde{\mathbf{f}}(\mathbf{h} \circ \alpha_{\mathcal{A}}(\mathbf{u}))p_t(\mathbf{h} \circ \alpha_{\mathcal{A}}(\mathbf{u}))] \cdot \left\{ \left((D\mathbf{h}(\mathbf{u}))^{-1} \right)^T \otimes \left(\frac{\partial\alpha_{\mathcal{A}}}{\partial u_1}, \frac{\partial\alpha_{\mathcal{A}}}{\partial u_2}, \dots, \frac{\partial\alpha_{\mathcal{A}}}{\partial u_{d-1}} \right) \right\}, \quad (71)$$

$$(72)$$

⁶ $\text{sign}(\mathbf{h})$ indicates whether \mathbf{h} changes the orientation of the parametrization. Since \mathbf{h} is assumed to be smooth and invertible (as it is an element of a group), its Jacobian is continuous in \mathbf{x} and cannot be zero. As a result, $\det D\mathbf{h}$ is either strictly greater than zero or less than zero over \mathbb{R}^d and thus $\text{sign}(\mathbf{h})$ is well-defined and is independent of the selection of \mathbf{x} .

which is

$$\left\{ p_t(\mathbf{h} \circ \alpha_{\mathcal{A}}(\mathbf{u})) \otimes \left(\frac{\partial \alpha_{\mathcal{A}}}{\partial u_1}, \frac{\partial \alpha_{\mathcal{A}}}{\partial u_2}, \dots, \frac{\partial \alpha_{\mathcal{A}}}{\partial u_{d-1}} \right) \right\} \cdot \left[\tilde{\mathbf{f}}(\alpha_{\mathcal{A}}(\mathbf{u})) - (Dh(\alpha_{\mathcal{A}}(\mathbf{u})))^{-1} \tilde{\mathbf{f}}(\mathbf{h} \circ \alpha_{\mathcal{A}}(\mathbf{u})) \right] = 0. \quad (73)$$

$$(74)$$

Since it is assumed that $p_t(\mathbf{x}) > 0$ for all $\mathbf{x} \in \mathbb{R}^d$, Eq (73) is simply

$$\otimes \left(\frac{\partial \alpha_{\mathcal{A}}}{\partial u_1}, \frac{\partial \alpha_{\mathcal{A}}}{\partial u_2}, \dots, \frac{\partial \alpha_{\mathcal{A}}}{\partial u_{d-1}} \right) \cdot \left[\tilde{\mathbf{f}}(\alpha_{\mathcal{A}}(\mathbf{u})) - (Dh(\alpha_{\mathcal{A}}(\mathbf{u})))^{-1} \tilde{\mathbf{f}}(\mathbf{h} \circ \alpha_{\mathcal{A}}(\mathbf{u})) \right] = 0. \quad (75)$$

As a result, for any point \mathbf{x} and any nonzero vector \mathbf{e} , we can choose proper \mathcal{A} and its surface parametrization $\alpha_{\mathcal{A}}(\mathbf{u})$ such that $\alpha_{\mathcal{A}}(\mathbf{u}) = \mathbf{x}$ and $\otimes \left(\frac{\partial \alpha_{\mathcal{A}}(\mathbf{u})}{\partial u_1}, \frac{\partial \alpha_{\mathcal{A}}(\mathbf{u})}{\partial u_2}, \dots, \frac{\partial \alpha_{\mathcal{A}}(\mathbf{u})}{\partial u_{d-1}} \right) = \lambda \mathbf{e}$ for some $\lambda \neq 0$. Hence, we have for all $\mathbf{x} \in \mathbb{R}^d$,

$$\tilde{\mathbf{f}}(\mathbf{x}) - (Dh(\mathbf{x}))^{-1} \tilde{\mathbf{f}}(\mathbf{h}(\mathbf{x})) = \mathbf{0}, \quad (76)$$

which is Eq (9).

Therefore, as $\tilde{\mathbf{f}}(\mathbf{x}, t) = \mathbf{f}(\mathbf{x}, t) - \frac{1}{2}g(t)^2 \nabla \log p_t(\mathbf{x})$, we have

$$Dh(\mathbf{x})[\mathbf{f}(\mathbf{x}, t) - \frac{1}{2}g(t)^2 \nabla \log p_t(\mathbf{x})] = \mathbf{f}(\mathbf{h}(\mathbf{x}), t) - \frac{1}{2}g(t)^2 \nabla \log p_t(\mathbf{h}(\mathbf{x})). \quad (77)$$

Besides, as p_t is $\mathcal{G}_{\mathcal{L}}$ -invariant, by Lem 1, we know

$$Dh(\mathbf{x})\nabla \log p_t(\mathbf{x}) = \nabla \log p_t(\mathbf{h}(\mathbf{x})). \quad (78)$$

Then, combining it with Eq (77), we get Eq (9).

(\Leftarrow) Assume p_0 is $\mathcal{G}_{\mathcal{L}}$ -invariant and $Dh(\mathbf{x}) \mathbf{f}(\mathbf{x}, t) = \mathbf{f}(\mathbf{h}(\mathbf{x}), t)$ for all $t \geq 0$ and $\mathbf{h} \in \mathcal{G}$. For any closed ball $B(\mathbf{x}_0, r)$ with $\mathbf{x}_0 \in \mathbb{R}^d$ and $r > 0$, by the Fokker-Planck equation, we have

$$\int_{B(\mathbf{x}_0, r)} p_t(\mathbf{x}) \, d\mathbf{x} = \int_{B(\mathbf{x}_0, r)} \left[p_0(\mathbf{x}) + \int_0^t \frac{\partial p_s(\mathbf{x})}{\partial s} \, ds \right] \, d\mathbf{x} \quad (79)$$

$$= \int_{B(\mathbf{x}_0, r)} \left[p_0(\mathbf{x}) + \int_0^t \left[-\nabla \cdot [\mathbf{f}(\mathbf{x}, t)p_t(\mathbf{x})] + \frac{1}{2}g(t)^2 \nabla \cdot (\nabla p_t(\mathbf{x})) \right] \, ds \right] \, d\mathbf{x} \quad (80)$$

$$= \int_{B(\mathbf{x}_0, r)} p_0(\mathbf{x}) \, d\mathbf{x} + \int_{B(\mathbf{x}_0, r)} \left[\int_0^t \left[-\nabla \cdot [\mathbf{f}(\mathbf{x}, t)p_t(\mathbf{x})] + \frac{1}{2}g(t)^2 \nabla \cdot (\nabla p_t(\mathbf{x})) \right] \, ds \right] \, d\mathbf{x} \quad (81)$$

$$= \int_{B(\mathbf{x}_0, r)} p_0(\mathbf{x}) \, d\mathbf{x} + \int_0^t \int_{B(\mathbf{x}_0, r)} \left[-\nabla \cdot [\mathbf{f}(\mathbf{x}, t)p_t(\mathbf{x})] + \frac{1}{2}g(t)^2 \nabla \cdot (\nabla p_t(\mathbf{x})) \right] \, d\mathbf{x} \, ds. \quad (82)$$

Therefore,

$$\frac{d}{dt} \int_{B(\mathbf{x}_0, r)} p_t(\mathbf{x}) \, d\mathbf{x} = \int_{B(\mathbf{x}_0, r)} \left[-\nabla \cdot [\mathbf{f}(\mathbf{x}, t)p_t(\mathbf{x})] + \frac{1}{2}g(t)^2 \nabla \cdot (\nabla p_t(\mathbf{x})) \right] \, d\mathbf{x} \quad (83)$$

$$= - \int_{B(\mathbf{x}_0, r)} \nabla \cdot [\mathbf{f}(\mathbf{x}, t)p_t(\mathbf{x})] \, d\mathbf{x} + \frac{1}{2}g(t)^2 \int_{B(\mathbf{x}_0, r)} \nabla \cdot (\nabla p_t(\mathbf{x})) \, d\mathbf{x}. \quad (84)$$

Likewise, by the Fokker-Planck equation, we also have

$$\frac{d}{dt} \underbrace{\int_{h(B(\mathbf{x}_0, r))} p_t(\mathbf{x}) \, d\mathbf{x}}_{\mathbf{I}} = - \underbrace{\int_{h(B(\mathbf{x}_0, r))} \nabla \cdot [\mathbf{f}(\mathbf{x}, t) p_t(\mathbf{x})] \, d\mathbf{x}}_{\mathbf{II}} + \frac{1}{2} g(t)^2 \underbrace{\int_{h(B(\mathbf{x}_0, r))} \nabla \cdot (\nabla p_t(\mathbf{x})) \, d\mathbf{x}}_{\mathbf{III}}. \quad (85)$$

Note that

$$\mathbf{I} = \int_{h(B(\mathbf{x}_0, r))} p_t(\mathbf{x}) \, d\mathbf{x} = \int_{B(\mathbf{x}_0, r)} p_t(\mathbf{h}(\mathbf{x})) |\det Dh(\mathbf{x})| \, d\mathbf{x} = \int_{B(\mathbf{x}_0, r)} p_t(\mathbf{h}(\mathbf{x})) \, d\mathbf{x} \quad (86)$$

$$\mathbf{III} = \int_{h(B(\mathbf{x}_0, r))} \nabla \cdot (\nabla p_t(\mathbf{x})) \, d\mathbf{x} = \int_{B(\mathbf{x}_0, r)} \nabla \cdot (\nabla p_t(\mathbf{h}(\mathbf{x}))) |\det Dh(\mathbf{x})| \, d\mathbf{x} = \int_{B(\mathbf{x}_0, r)} \nabla \cdot (\nabla p_t(\mathbf{h}(\mathbf{x}))) \, d\mathbf{x}. \quad (87)$$

And for \mathbf{II} , according to theorem 1, we have

$$\mathbf{II} = \int_{h(B(\mathbf{x}_0, r))} \nabla \cdot [\mathbf{f}(\mathbf{x}, t) p_t(\mathbf{x})] \, d\mathbf{x} = \int_{\partial h(B(\mathbf{x}_0, r))} [\mathbf{f}(\mathbf{x}, t) p_t(\mathbf{x})] \cdot \mathbf{n} \, d\mathcal{S}. \quad (88)$$

As h is a linear isometry, by Lem 4, $|\det Dh| = 1$. According to Lem 3, for a smooth function $\boldsymbol{\eta} : \mathbb{R}^d \rightarrow \mathbb{R}^d$, we have

$$\int_{\partial h(B(\mathbf{x}_0, r))} \boldsymbol{\eta}(\mathbf{x}) \cdot \mathbf{n} \, d\mathcal{S} = \int_{\partial B(\mathbf{x}_0, r)} (Dh(\mathbf{x}))^{-1} \boldsymbol{\eta}(\mathbf{h}(\mathbf{x})) \cdot \mathbf{n} \, d\mathcal{S}. \quad (89)$$

Therefore,

$$\mathbf{II} = \int_{\partial B(\mathbf{x}_0, r)} [(Dh(\mathbf{x}))^{-1} \mathbf{f}(\mathbf{h}(\mathbf{x}), t) p_t(\mathbf{h}(\mathbf{x}))] \cdot \mathbf{n} \, d\mathcal{S}. \quad (90)$$

As it is assumed that $Dh(\mathbf{x}) \mathbf{f}(\mathbf{x}, t) = \mathbf{f}(\mathbf{h}(\mathbf{x}), t)$,

$$\mathbf{II} = \int_{\partial B(\mathbf{x}_0, r)} [\mathbf{f}(\mathbf{x}, t) p_t(\mathbf{h}(\mathbf{x}))] \cdot \mathbf{n} \, d\mathcal{S} = \int_{B(\mathbf{x}_0, r)} \nabla \cdot [\mathbf{f}(\mathbf{x}, t) p_t(\mathbf{h}(\mathbf{x}))] \, d\mathbf{x}. \quad (91)$$

Combining Eq (85), Eq (86), Eq (87) and Eq (91), we have

$$\frac{d}{dt} \int_{B(\mathbf{x}_0, r)} p_t(\mathbf{h}(\mathbf{x})) \, d\mathbf{x} = \int_{B(\mathbf{x}_0, r)} \nabla \cdot [\mathbf{f}(\mathbf{x}, t) p_t(\mathbf{h}(\mathbf{x}))] \, d\mathbf{x} + \frac{1}{2} g(t)^2 \int_{B(\mathbf{x}_0, r)} \nabla \cdot (\nabla p_t(\mathbf{h}(\mathbf{x}))) \, d\mathbf{x}. \quad (92)$$

Then subtracting Eq (92) from Eq (84), we have

$$\frac{d}{dt} \int_{B(\mathbf{x}_0, r)} p_t(\mathbf{x}) - p_t(\mathbf{h}(\mathbf{x})) \, d\mathbf{x} = - \int_{B(\mathbf{x}_0, r)} \nabla \cdot [\mathbf{f}(\mathbf{x}, t) (p_t(\mathbf{x}) - p_t(\mathbf{h}(\mathbf{x})))] \, d\mathbf{x} \quad (93)$$

$$+ \frac{1}{2} g(t)^2 \int_{B(\mathbf{x}_0, r)} \nabla \cdot (\nabla (p_t(\mathbf{x}) - p_t(\mathbf{h}(\mathbf{x})))) \, d\mathbf{x}. \quad (94)$$

Since all three integrands are assumed continuous in \mathbf{x} , applying the mean value theorem followed by taking the limit $r \rightarrow 0$ yields the following ODE

$$\frac{d}{dt} (p_t(\mathbf{x}_0) - p_t(\mathbf{h}(\mathbf{x}_0))) = -\nabla \cdot [\mathbf{f}(\mathbf{x}_0, t) (p_t(\mathbf{x}_0) - p_t(\mathbf{h}(\mathbf{x}_0)))] + \frac{1}{2} g(t)^2 \nabla \cdot \nabla (p_t(\mathbf{x}_0) - p_t(\mathbf{h}(\mathbf{x}_0))). \quad (95)$$

Let $\delta(\mathbf{x}, t) = p_t(\mathbf{x}) - p_t(\mathbf{h}(\mathbf{x}))$. The ODE can be rewritten as

$$\frac{d}{dt} \delta(\mathbf{x}, t) = -\nabla \cdot [\mathbf{f}(\mathbf{x}_0, t) \delta(\mathbf{x}, t)] + \frac{1}{2} g(t)^2 \nabla \cdot \nabla (\delta(\mathbf{x}, t)) \quad (96)$$

with the boundary condition $\delta(\mathbf{x}, 0) = p_0(\mathbf{x}) - p_0(\mathbf{h}(\mathbf{x})) = 0$ (due to that fact that p_0 is $\mathcal{G}_{\mathcal{L}}$ -invariant and Lem 6).

It is easy to check that $\delta(\mathbf{x}, t) = 0$ for all $t \geq 0$ is a solution to the ODE. Additionally, as its terms are all continuous in \mathbf{x} and t , the solution is unique. Therefore, we conclude that $\delta(\mathbf{x}, t) = 0$ for all $t \geq 0$ and $\mathbf{x} \in \mathbb{R}^d$. Namely, $p_t(\mathbf{x}) = p_t(\mathbf{h}(\mathbf{x}))$ for all \mathbf{x} and t . According to Lem 6, this implies p_t is \mathcal{G} -invariant for all $t \geq 0$. ■

Corollary 1 *Assume the drift term takes the form $\mathbf{f}(\mathbf{x}, t) = \mathbf{x}f(t)$ for some scalar function $f : \mathbb{R} \rightarrow \mathbb{R}$. Then for any group $\mathcal{G}_{\mathcal{L}}$ composed of linear isometries, if p_t is $\mathcal{G}_{\mathcal{L}}$ -invariant at $t = 0$, then it is $\mathcal{G}_{\mathcal{L}}$ -invariant for all $t \geq 0$.*

Proof: Since for all $\mathbf{h} \in \mathcal{G}_{\mathcal{L}}$, there exists some $A \in \mathbb{R}^{d \times d}$ such that $\mathbf{h}(\mathbf{x}) = A\mathbf{x}$, and thus, we have $D\mathbf{h}(\mathbf{x}) = A$. Then we have for all $t \geq 0$ and $\mathbf{x} \in \mathbb{R}^d$,

$$D\mathbf{h}(\mathbf{x}) \mathbf{f}(\mathbf{x}, t) = A\mathbf{f}(\mathbf{x}, t) = A\mathbf{x}f(t) = (A\mathbf{x})f(t) = \mathbf{f}(A\mathbf{x}, t). \quad (97)$$

Therefore, according to Prop 1, we conclude that p_t is $\mathcal{G}_{\mathcal{L}}$ -invariant for all $t \geq 0$. ■

A.4 Techniques to Obtain $\mathcal{G}_{\mathcal{L}}$ -equivariant Functions

Lemma 7 *For any function $\mathbf{r} : \mathbb{R}^d \rightarrow \mathbb{R}^d$ and linear operator group $\mathcal{G}_{\mathcal{L}}$,*

$$\tilde{\mathbf{r}}(\mathbf{x}) = \frac{1}{|\mathcal{G}_{\mathcal{L}}|} \sum_{\mathbf{h} \in \mathcal{G}_{\mathcal{L}}} A_{\mathbf{h}^{-1}} \mathbf{r}(A_{\mathbf{h}}\mathbf{x}) \quad (98)$$

is $\mathcal{G}_{\mathcal{L}}$ -equivariant, where $|\mathcal{G}_{\mathcal{L}}|$ denotes the number of elements in $\mathcal{G}_{\mathcal{L}}$ and $A_{\mathbf{h}}$ is the matrix such that $\mathbf{h}(\mathbf{x}) = A_{\mathbf{h}}\mathbf{x}$.

Proof: It is sufficient to show, for $\mathbf{h}' \in \mathcal{G}_{\mathcal{L}}$, we have $\tilde{\mathbf{r}}(A_{\mathbf{h}'}\mathbf{x}) = A_{\mathbf{h}'}\tilde{\mathbf{r}}(\mathbf{x})$. Note that

$$\tilde{\mathbf{r}}(A_{\mathbf{h}'}\mathbf{x}) = \frac{1}{|\mathcal{G}_{\mathcal{L}}|} \sum_{\mathbf{h} \in \mathcal{G}_{\mathcal{L}}} A_{\mathbf{h}^{-1}} \mathbf{r}(A_{\mathbf{h}}A_{\mathbf{h}'}\mathbf{x}) = \frac{1}{|\mathcal{G}_{\mathcal{L}}|} \sum_{\mathbf{h} \in \mathcal{G}_{\mathcal{L}}} A_{\mathbf{h}^{-1}} \mathbf{r}(A_{\mathbf{h} \circ \mathbf{h}'}\mathbf{x}) = \frac{1}{|\mathcal{G}_{\mathcal{L}}|} \sum_{\mathbf{h}'' \in \mathcal{G}_{\mathcal{L}}} A_{\mathbf{h}'' \circ (\mathbf{h}')^{-1}}^{-1} \mathbf{r}(A_{\mathbf{h}''}\mathbf{x}) \quad (99)$$

with $\mathbf{h}'' = \mathbf{h} \circ \mathbf{h}'$. As

$$A_{\mathbf{h}'' \circ (\mathbf{h}')^{-1}}^{-1} = [A_{\mathbf{h}'' \circ (\mathbf{h}')^{-1}}]^{-1} = [A_{\mathbf{h}''}A_{(\mathbf{h}')^{-1}}]^{-1} = [A_{\mathbf{h}''}A_{(\mathbf{h}')^{-1}}]^{-1} = A_{\mathbf{h}'}A_{\mathbf{h}''}^{-1}, \quad (100)$$

we have

$$\tilde{\mathbf{r}}(A_{\mathbf{h}'}\mathbf{x}) = A_{\mathbf{h}'} \frac{1}{|\mathcal{G}_{\mathcal{L}}|} \sum_{\mathbf{h}'' \in \mathcal{G}_{\mathcal{L}}} A_{\mathbf{h}''}^{-1} \mathbf{r}(A_{\mathbf{h}''}\mathbf{x}) = A_{\mathbf{h}'}\tilde{\mathbf{r}}(\mathbf{x}), \quad (101)$$

which completes the proof. ■

B Group Invariant Weight Tied Convolutional Kernels

As stated in Sec 5, we currently limit our attention to linear isometry groups $\mathcal{G}_{\mathcal{L}}$. In this setting, we can directly impose $\mathcal{G}_{\mathcal{L}}$ -equivariance into the diffusion model by constructing specific CNN kernels.

In particular, for a given linear group $\mathcal{G}_{\mathcal{L}}$ we can construct a group equivariant convolutional kernel $\mathbf{k} \in \mathbb{R}^{d \times d}$, of the form

$$\mathbf{k} = \begin{array}{|c|c|c|c|} \hline k_{1,1} & k_{1,2} & \cdots & k_{1,d} \\ \hline \vdots & \vdots & \ddots & \vdots \\ \hline \vdots & \vdots & & \vdots \\ \hline k_{d-1,1} & k_{d-1,2} & \cdots & k_{d-1,d} \\ \hline k_{d,1} & k_{d,2} & \cdots & k_{d,d} \\ \hline \end{array}, \quad (102)$$

such that

$$\mathbf{h}(\mathbf{k} * \mathbf{x}) = \mathbf{k} * \mathbf{h}(\mathbf{x}) \quad (103)$$

for any $h \in \mathcal{G}_{\mathcal{L}}$ and $\mathbf{x} \sim p_{data}$ by constraining the individual kernel values to obey a system of equalities set by the group invariance condition:

$$\mathbf{h}(\mathbf{k}) = \mathbf{k}, \quad (104)$$

for all $\mathbf{h} \in \mathcal{G}_{\mathcal{L}}$.⁷

Example: Vertical flipping. A concrete example, which was discussed Sec 3.2, is to consider the group $\mathcal{G} = \{f_x, \mathbf{e}\}$ where f_x is a vertical flipping operation with $f_x^{-1} = f_x$. A convolutional kernel $\mathbf{k} \in \mathbb{R}^{3 \times 3}$ constrained to be equivariant to actions from this group would take the form:

$$\mathbf{k} = \begin{array}{|c|c|c|} \hline d & a & d \\ \hline e & b & e \\ \hline f & c & f \\ \hline \end{array} \quad (105)$$

It should be clear given the form of \mathbf{k} that

$$f_x(\mathbf{k} * \mathbf{x}) = \mathbf{k} * f_x(\mathbf{x}) \quad (106)$$

and consequently also for f_x^{-1} , as desired. Likewise, we also present the weight-tied kernels for C_4 and D_4 .

Example: The C_4 cyclic and D_4 dihedral group. Recall that the C_4 cyclic group is composed of planar 90 deg rotations about the origin, and can be denoted as $C_4 = \{\mathbf{e}, r_1, r_2, r_3\}$ where r_i represents a rotation of $i \times 90$ deg. Taking a convolutional kernel $\mathbf{k} \in \mathbb{R}^{5 \times 5}$ and constraining it to be C_4 -equivariant results in \mathbf{k} being of the form:

$$\mathbf{k} = \begin{array}{|c|c|c|c|c|} \hline a & b & c & d & a \\ \hline d & e & f & e & b \\ \hline c & f & g & f & c \\ \hline b & e & f & e & d \\ \hline a & d & c & b & a \\ \hline \end{array}. \quad (107)$$

The D_4 dihedral group can then be “constructed” from C_4 by adding the vertical flipping operation from the past example; that is, $D_4 = \{\mathbf{e}, r_1, r_2, r_3, f_x, f_x \circ r_1, f_x \circ r_2, f_x \circ r_3\}$. This requires further constraints to \mathbf{k} so that

$$\mathbf{k} = \begin{array}{|c|c|c|c|c|} \hline a & b & c & b & a \\ \hline b & e & f & e & b \\ \hline c & f & g & f & c \\ \hline b & e & f & e & b \\ \hline a & b & c & b & a \\ \hline \end{array}. \quad (108)$$

⁷We slightly abused the notation \mathbf{h} by treating kernel \mathbf{k} as an image. What we mean is that: to achieve equivariance of a CNN under a particular image transformation (such as rotation), we can simply pick a kernel \mathbf{k} that remains invariant under this transformation.

Naturally, constraining convolutional kernels in this fashion has the advantage of reducing the number of model parameters – with a possible loss in expressiveness when the kernel size is relatively small in comparison to the size of the group and structure of the data. For a more general discussion on \mathcal{G} -equivariant convolutional kernels in the context of CNNs we refer the reader to Cohen and Welling (2016) and Knigge et al. (2022).

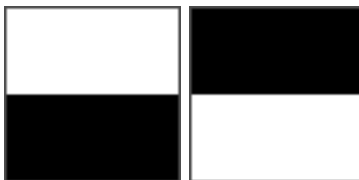
C Selections of ϕ to Make the Noise Sequence Equivariant

In Sec 5.2, we showed that we can construct an equivariant noisy sequence $\{\epsilon_i\}_{i=1}^n$ with respect to some $\mathbf{x}_n \sim q(\mathbf{x})$ by constructing a function $\phi : \mathbb{R}^d \rightarrow \mathbb{R}^d$ such that:

1. For all $\mathbf{h} \in \mathcal{G}_{\mathcal{L}}$, $\mathbf{x} \sim q$ or $\mathbf{x} \sim \mathcal{N}(\mathbf{0}, I)$, $\phi(A_{\mathbf{h}}\mathbf{x}) = A_{\mathbf{h}}\phi(\mathbf{x})$ almost surely;
2. For all $\mathbf{x}, \mathbf{y} \in \mathbb{R}^d$, there exists a unique $\mathbf{h} \in \mathcal{G}_{\mathcal{L}}$ such that $\phi(\mathbf{x}) = A_{\mathbf{h}}\phi(\mathbf{y})$.

Here, we present some choices of ϕ for some common linear operator groups for 2D images.

Example: Vertical flipping. The function ϕ_v can be chosen to output either of two images:



Specifically, if the input image \mathbf{x} has the max value on the upper half of the image, ϕ returns the left plot; otherwise, the right one. (Here, we assume it is almost surely that the max value cannot appear in both halves.)

It is obvious that if the input is flipped vertically, the output will be flipped in the same way. Therefore, the first condition is satisfied. For the second one, if $\phi_v(\mathbf{x})$ and $\phi_v(\mathbf{y})$ have the same output, \mathbf{h} is the identity operator; otherwise, \mathbf{h} is the vertical flipping. For multichannel inputs, ϕ can be applied to each channel independently.

Applying the same idea, we can derive the corresponding ϕ_h for horizontal flipping.

Example: C_4 cyclic group. We can use a similar idea to derive ϕ_{C_4} for C_4 cyclic that is composed of planar 90 deg rotations about the origin. In this case, ϕ_{C_4} has four possible outputs



such that ϕ_{C_4} assigns the quadrant white if the input has the max value in that quadrant. (Here, we assume it is almost surely that the max value cannot appear in multiple quadrants.) Then, it is straightforward to see that ϕ_{C_4} satisfies the two conditions of ϕ .

Example: D_4 dihedral group. As we have mentioned in appx B, the D_4 dihedral group can be “constructed” from C_4 by adding the vertical flipping operation. As a result, we can combine ϕ_v and ϕ_{C_4} to construct the corresponding ϕ_{D_4} for D_4 . Assume that ϕ_v assigns one to the elements corresponding to the white pixels and zero to the ones associated with the black. Likewise, let ϕ_{C_4} assign two to the elements corresponding to the white pixels and zero to the rest. Then we define $\phi_{D_4} = \phi_v + \phi_{C_4}$. It is easy to check that both ϕ_v and ϕ_{D_4} satisfy the first condition of ϕ for all $\mathbf{h} \in D_4$ (i.e., vertical flipping, rotation, and their composition). We also note that the range ϕ_{D_4} contains eight distinct elements. Starting from one element, we get all the elements by applying one of the eight operators in $D_4 = \{e, r_1, r_2, r_3, f_x, f_x \circ r_1, f_x \circ r_2, f_x \circ r_3\}$, which suggests ϕ_{D_4} satisfies the second condition.

D Model Implementation Details

The implementation details and hyperparameters used while training the models presented in Sec 6 over the listed datasets are given below.

All models are trained using the Adam optimizer Kingma and Ba 2015 with learning rate $\eta = 0.0001 \cdot 0.0002$, and weight decay rate of $\gamma = 0.0$; separately, we make use of the exponential moving average (EMA) of the model weights Eq (16) with $\mu = 0.999, 0.9999, 0.9999432189950708$, which are the values commonly used when training diffusion models.

As we discuss a selection of different implementations in Sec 5, a brief summary of the different training objectives is provided below for reference, the individual value objective terms can be found in the aforementioned section.

$$\mathcal{L}(\boldsymbol{\theta}) = \mathbb{E} \left[\left\| \mathbf{s}_{\boldsymbol{\theta}}(\mathbf{x}_t, t) - \nabla_{\mathbf{x}_t} \log p(\mathbf{x}_t | \mathbf{x}_0) \right\|^2 \right] \quad (109)$$

$$\mathcal{L}_{OC}(\boldsymbol{\theta}) = \mathbb{E} \left[\left\| \tilde{\mathbf{r}}(\mathbf{x} - \nabla_{\mathbf{x}_t} \log p(\mathbf{x}_t | \mathbf{x}_0)) \right\|^2 \right] \quad (110)$$

$$\mathcal{L}_R(\boldsymbol{\theta}) = \mathcal{L}(\boldsymbol{\theta}) + \mathcal{R}(\boldsymbol{\theta}, \bar{\boldsymbol{\theta}}) \quad (111)$$

D.1 Rotated MNIST

For the Roatated MNIST datasets, the diffusion models are configured using the following model parameters: dropout rate $d = 0.1$.

Model	Loss	Batch	Cond.	Aug	Attn. res.	Num. Ch.	Num. Heads	Ch. Scal.	Scale Shift
SPDiff	\mathcal{L}	32	True	True	8	128	16	1,2,2	True
SPDiff+WT	\mathcal{L}	32	True	False	8	128	16	1,2,2	True
SPDiff+OC	\mathcal{L}_{OC}	32	True	True	8	128	16	1,2,2	True
SPDiff+Reg	\mathcal{L}_R	32	True	True	8	128	16	1,2,2	True
SPDiff+Reg+OC	$\mathcal{L}_{OC} + R$	32	True	True	8	128	16	1,2,2	True

D.2 LYSTO

For the LYSTO dataset, the diffusion models are configured using the following model parameters: dropout rate $d = 0.1$.

Model	Loss	Batch	Cond.	Aug	Attn. res.	Num. Ch.	Num. Heads	Ch. Scal.	Scale Shift
SPDiff	\mathcal{L}	32	True	True	32,16,8	128	64	1,2,2,2	True
SPDiff+WT	\mathcal{L}	32	True	False	32,16,8	128	64	1,2,2,2	True
SPDiff+OC	\mathcal{L}_{OC}	32	True	True	32,16,8	128	64	1,2,2,2	True
SPDiff+Reg	\mathcal{L}_R	32	True	True	32,16,8	128	64	1,2,2,2	True
SPDiff+Reg+OC	$\mathcal{L}_{OC} + R$	32	True	True	32,16,8	128	64	1,2,2,2	True

We refer the reader to the reader to Appx.G. of Birrell et al. (2022) for the implementation details and training parameters used to produce the results of SP-GAN reported in Sec 6.

E Sample Images

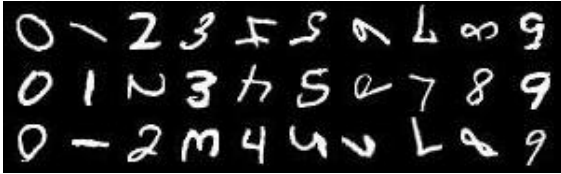
Here, we include a collection of generated image samples from the models discussed within the paper across the various datasets in Section 6.



(a) Reference C_4 rotated MNIST images.



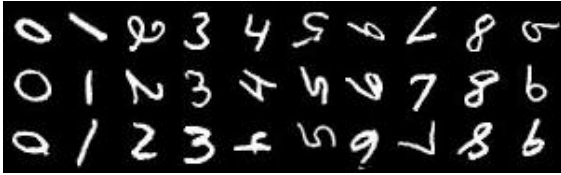
(b) Images generated from SP-GAN.



(c) Images generated from SPDiff+Aug.



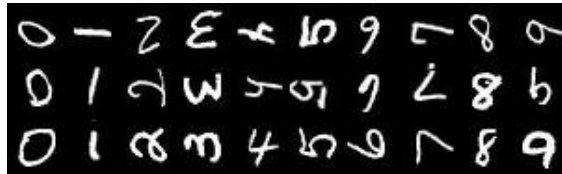
(d) Images generated from SPDiff+WT



(e) Images generated from SPDiff+OC

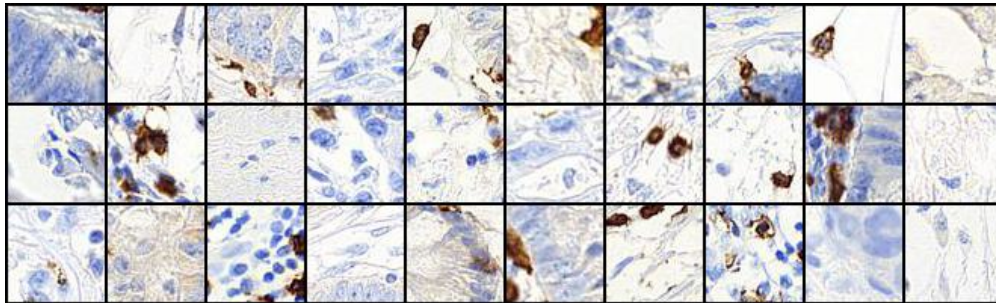


(f) Images generated from SPDiff+Reg.

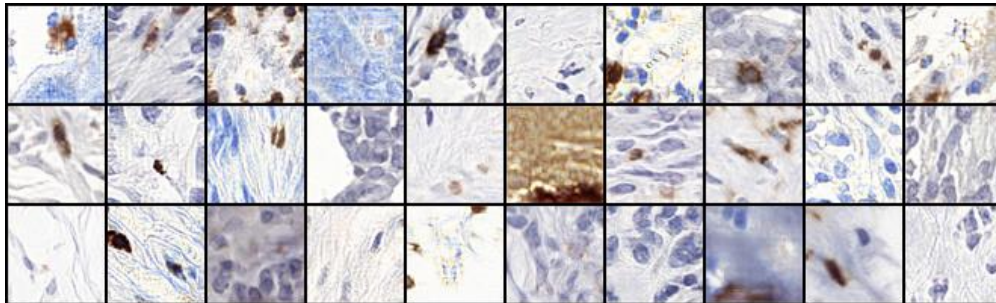


(g) Images generated from SPDiff+Reg+OC.

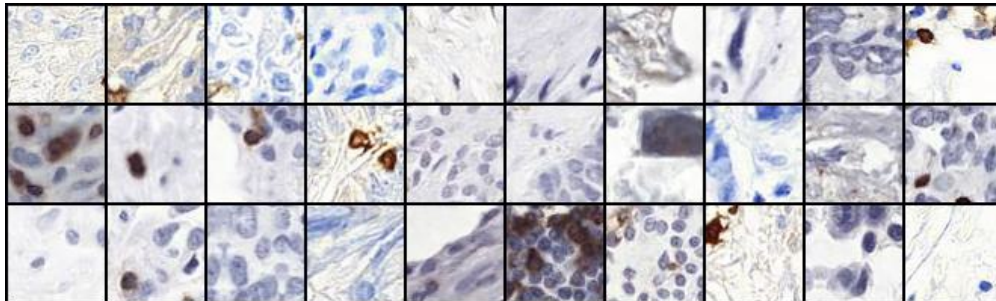
Figure 6: Sample comparison between models trained on the Rotated MNIST 28x28x1 dataset as described in Sec 6.



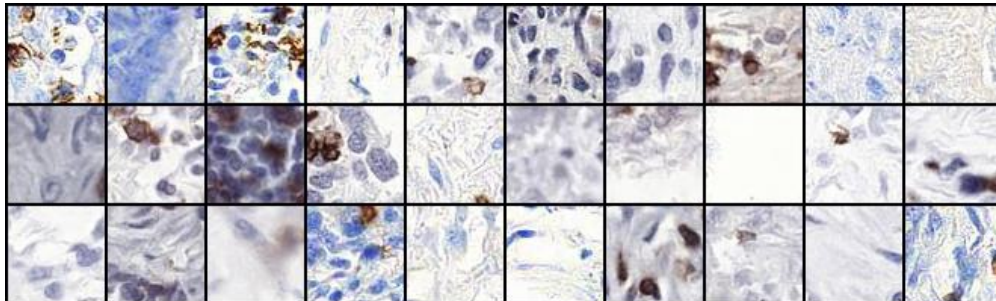
(a) Reference images.



(b) Images generated from SP-GAN.

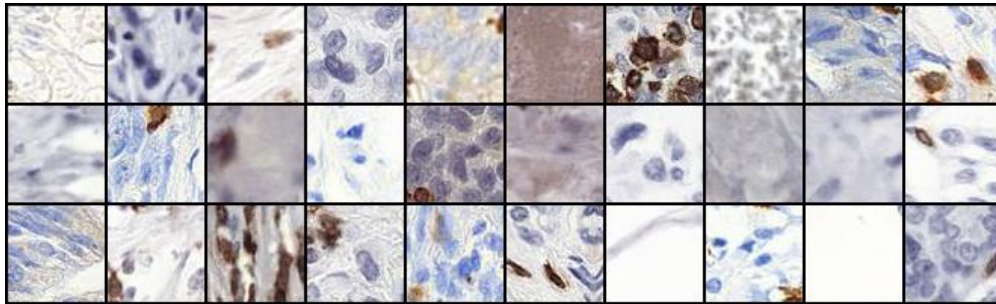


(c) Images generated from SPDiff+Aug

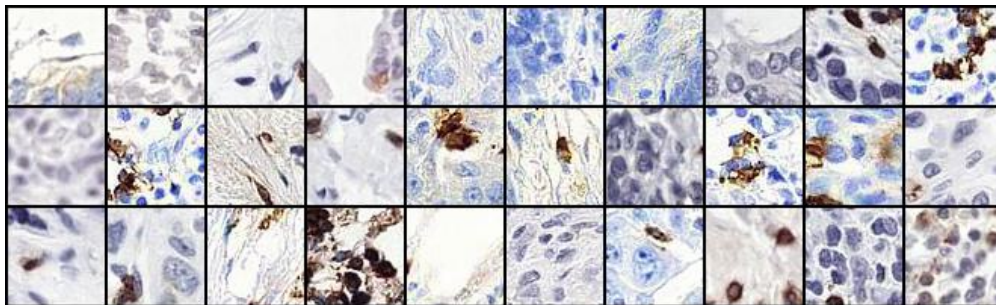


(d) Images generated from SPDiff+WT.

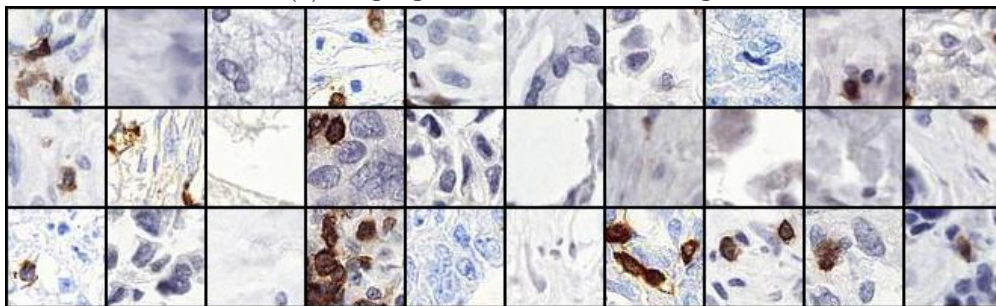
Figure 7: Sample comparison between models trained on the LYSTO 64x64x3 dataset from Sec 6.



(a) Images generated from SPDiff+OC



(b) Images generated from SPDiff+Reg.



(c) Images generated from SPDiff+Reg+OC.

Figure 8: Sample comparison between models trained on the LYSTO 64x64x3 dataset from Sec 6. (Continued.)